PhD School in Industrial Engineering

PhD in Energy Engineering and
Innovative Industrial Technologies

XXVI cycle (2011-2013)

On the Update of a Steam Turbine Industrial Design Procedure

PhD student: Eng. Federica Sazzini

Supervisor: Prof. Andrea Arnone

Co-supervisor: Eng. Filippo Rubechini

Co-supervisor: Eng. Lorenzo Arcangeli

Coordinator: Prof. Maurizio De Lucia

Florence, January 2014

When the winds of change
blow, some people
build walls and
others build windmills

Chinese proverb

Aknowledgments

Vorrei esprimere il mio ringraziamento al Professor Arnone per avermi scelta per affrontare questo impegnativo lavoro di ricerca.
Vorrei ringraziare i miei colleghi del T-Group, per la professionalità e l'affiatamento che li contraddistingue. Grazie per tutto quello che mi avete insegnato. Un grazie speciale a Matteo, perchè oltre a un collega ho trovato un caro amico.

Grazie a tutti i ragazzi del reparto Turbine a vapore di Nuovo Pignone - GE Oil & Gas, per la battuta sempre pronta e perchè per voi lavorare insieme non è solo dividere lo stesso spazio. In particolare, un grande grazie a Lorenzo Arcangeli, per la fiducia e il rispetto che mi hai sempre dimostrato. Un piccolo saluto a Daniele, che ha incrociato il mio cammino per un breve periodo e ha lasciato il ricordo della persona buona quale era.

In questi tre anni molto è cambiato, mi ritrovo diversa da come ero partita, e spero migliore. Grazie ai miei affetti, ad Alessandro, per la luce che hai visto in me nei momenti bui, a mia mamma, per tutto quello che hai fatto, giusto o sbagliato, perchè ci hai provato.

Vorrei ringraziare tutti i miei famtasmi, vi sento ancora tutti qui.

Infine, un grazie a tutte le persone che dividono qualcosa con me, perchè sto imparando a lasciarvi entrare, e tutto diventa più bello.

Introduction

The present PhD Thesis addresses the subject of steam turbine design and analysis.

Steam turbines are used in a huge range of applications: from mechanical drive applications, e.g.driving pumps and compressors, to power generation applications.

The design procedure of a turbomachine is a very complex engineering operation, involving thermodynamic, aerodynamic, technological and structural aspects. At the same time the time to market is of crucial importance for industry, hence fast and reliable tools for design are required.

Moreover, steam turbines are faithful partners to the process industries. They have proven their reliability and keep pace with every demand of capacity and speed. The design process hence has to be fast, reliable and capable to respond to the most different requirements in terms of operating range and power.

The focus of the present thesis is the review of the steam turbines design process carried out in Nuovo Pignone-GE Oil&Gas.

This process is based on a one-dimensional design tool. The turbines designed with the aid of this tool are composed of:

- 1 or 2 impulse stages for the steam mass flow partialization

- 1 or more drums with 50% reaction stages
- 1 condensing drum

Figure 1: GE-Nuovo Pignone Steam Turbine

The turbines output of this tool have at the moment unsatisfactory efficiency levels. The object of the present research is hence the review of the design procedure of the 50% reaction stages, seeking higher efficiencies. Given the deep integration of the one-dimensional tool with all the subsequent phases of the product development, this must remain the main instrument of the design process. Furthermore its integration with the subsequent phases of the industrial product development have to be preserved.

The thesis is organized as follows:

- Chapter 1: A brief description of the state of the art of turbine design methodologies
- Chapter 2: A brief description of the existing design tool
- Chapter 3: How the efficiency increase has been pursued and how it has been realized through the modified design procedure

- Chapter 4: How the integration of the tool with the subsequent phases of the product development has been conserved and enhanced
- Chapter 5: Results and examples of turbines output of the new design procedure

Nomenclature

AR	Aspect Ratio, $\frac{H}{C}$
H	Blade Heigth
C	Blade Chord
Z	Number of Stages
RR	Radius Ratio, $\frac{R_{TIP}}{R_{HUB}}$
Re	Reynolds Number
F_c	Centrifugal Force

Greek

φ	Flow Coefficient, $\frac{c_x}{U}$
ψ	Load coefficient, $\frac{\Delta H_0}{\frac{U^2}{2}}$
ξ	Stagger Angle
σ	Stress [MPa]
ζ	Loss Coefficient, $1 - (\frac{c}{c_{is}})^2$
η	Total-to-Total Efficiency
ΔH	Enthalpy Drop

Acronyms

CFD	Computational Fluid Dynamics
LE	Leading Edge
TE	Trailing Edge
BEP	Best Efficiency Point
FEM	Finite Element Method

Subscripts

sec	Secondary
tot	Total
p	Profile
all	Allowable

Contents

List of Figures

Chapter 1

State of the Art

This chapter provides a description of the state of the art of the methodologies for turbine design

1.1 Steam Turbine

A steam turbine is a device that extracts thermal energy from pressurized steam and uses it to do mechanical work on a rotating output shaft.
Its modern manifestation was invented by Sir Charles Parsons in 1884. This first model was connected to a dynamo that generated 7.5kW of electricity. The invention of Parsons' steam turbine made cheap and plentiful electricity possible and revolutionized marine transport and naval warfare. Parsons' design was a reaction type.
A number of other variations of turbines have been developed that work effectively with steam. The De Laval turbine (invented by Gustaf de Laval) accelerated the steam to full speed before running it against a turbine blade.
One of the founders of the modern theory of steam and gas turbines was also Aurel Stodola, a Slovak physicist and engineer and professor at Swiss Polytechnic Institute (now ETH)

in Zurich. His mature work was "Die Dampfturbinen und ihre Aussichten als Wärmekraftmaschinen"([11]). In 1922, in Berlin, was published another important book: "Dampf und Gas-Turbinen"([12]).

The Brown-Curtis turbine, an impulse type, which had been originally developed and patented by the U.S. company International Curtis Marine Turbine Company, was developed in the 1900s in conjunction with John Brown&Company.

It was used in John Brown-engined merchant ships and warships, including liners and Royal Navy warships.

Steam turbines are made in a variety of sizes ranging from smaller than 0.75kW units used as mechanical drives for pumps, compressors and other shaft driven equipment, to 1,500 MW turbines used to generate electricity.

There are several classifications for modern steam turbines. To maximize turbine efficiency the steam is expanded, doing work, in a number of stages. These stages are characterized by how the energy is extracted from them and are known as either **impulse** or **reaction turbines**. Most steam turbines use a mixture of the reaction and impulse designs: each stage behaves as either one or the other, but the overall turbine uses both. Typically, higher pressure sections are reaction type and lower pressure stages are impulse type.

1.1.1 Impulse turbine

An impulse turbine has fixed nozzles that orient the steam flow into high speed jets. These jets contain significant kinetic energy, which is converted into shaft rotation by the rotor blades, as the steam jet changes direction. A pressure drop occurs across only the stationary blades, with a net increase in steam velocity across the stage. As the steam flows through

the nozzle its pressure falls from inlet pressure to the exit pressure.
Due to this high ratio of expansion of steam, the steam leaves the nozzle with a very high velocity. The steam leaving the moving blades has a large portion of the maximum velocity of the steam when leaving the nozzle. The loss of energy due to this higher exit velocity is commonly called the carry over velocity or leaving loss. The law of momentum states that the sum of the moments of external forces acting on a fluid which is temporarily occupying the control volume is equal to the net time change of angular momentum flux through the control volume.

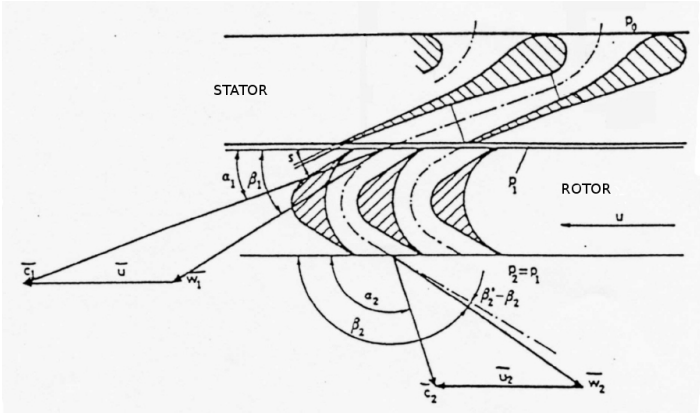

Figure 1.1: Impulse Stage

1.1.2 Reaction turbine

In the reaction turbine, the rotor blades themselves are arranged to form convergent nozzles. This type of turbine makes use of the reaction force produced as the steam accelerates through the nozzles formed by the rotor. Steam is directed

onto the rotor by the fixed vanes of the stator. It leaves the stator as a jet that fills the entire circumference of the rotor. The steam then changes direction and increases its speed relative to the speed of the blades. A pressure drop occurs across both the stator and the rotor, with steam accelerating through the stator and decelerating through the rotor, with no net change in steam velocity across the stage but with a decrease in both pressure and temperature, reflecting the work performed in the driving of the rotor.

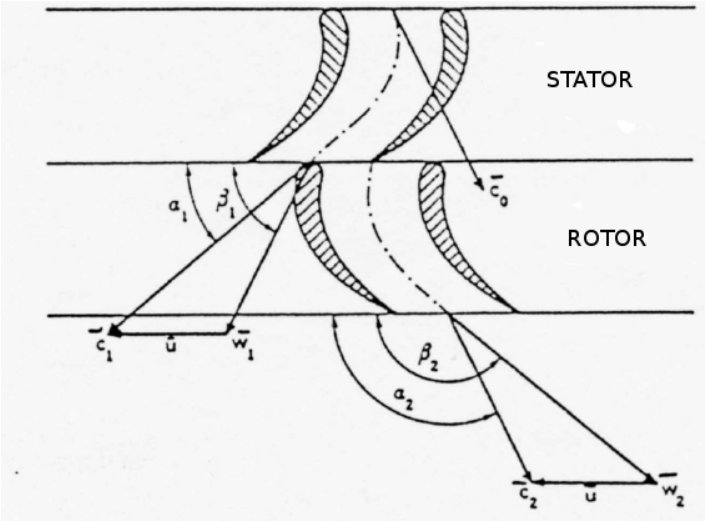

Figure 1.2: Reaction Stage

1.2 Methodologies for Turbine Design

In the early development of turbines, many empirical design rules were used. At the beginning of the 1950s turbine design relied substantially on empirical correlations of data. Turbine design has almost always involved mean line analysis or simple radial equilibrium theory together with empirical information on blade section performance. Efficiency was estimated using empirical expressions for basic two-dimensional loss, secondary loss and clearance loss.

At the beginning of the 1960s a strong effort has been made in the analytical research both in two directions:

- Direct problem: Solving the flow through cascades of a given shape
- Indirect problem: Obtaining the required blade shape once the surface velocity distribution has been given

We can cite:

- Blade to Blade flow analysis: analysis of the two-dimensional potential flow in given turbine cascades
- Through-Flow methods: these represented the start of the practical application of CFD to turbomachinery design. These methods still require empirical input for the blade row loss and deviation but allow designs with arbitrary vortex distribution to be developed. These methods remain the backbone of the modern compressor and turbine design process. They are used both in the design mode, where enthalpy or angular momentum changes are specified and the flow angles are sought, and in the analysis mode where specified machine geometry is analyzed to predict performance.

Modern turbomachinery design relies almost completely on CFD to develop blade sections. What CFD really provides

is the ability to exploit the three dimensional nature of the flow to control undesirable features such as strong secondary flows in turbines.

Simple methods with empirical inputs are still needed for the mean-line design and for through-flow calculation and it is often emphasised by experienced designers that if the one-dimensional design in not correct then no amount of CFD will produce a good design.

1.3 Design methods for routine design

As aforementioned in the turbine design we can face two different problems:

- Direct problem: Solving the flow through cascades of a given shape
- Indirect problem: Obtaining the required blade shape once the surface velocity distribution has been given

The direct problem can be faced with a growing level of precision with:

- Mean line analysis and empirical input for the blade row loss and deviation
- Through-Flow methods with empirical input for the blade row loss and deviation
- CFD methods

CFD calculation for a complete turbine are still too time consuming for routine design, while the first two methods are currently used for industrial design. Hence, simple methods with empirical inputs are still needed for the mean-line design and for through flow calculation or an entire turbine.

Chapter 2

Analysis of the Existing Design Tool

This chapter provides a description of the existing industrial tool for steam turbine design

The analysis of the existing tool has been an essential step of the present work. In fact, due to industrial needs, it was necessary to maintain the existing tool as the main one for the turbine design.

This tool performs both a thermodynamic and mechanical design. Given few inputs selected by the design engineer with a front-end interface the tool designs a complete 50% reaction drum.

The analysis carried out can be divided into:

1. Mean line thermodynamic analysis

2. Mechanical verifications

In fig 2.1 it is reported a schematic flowchart of the code. As it can be seen, the thermodynamic design and the me-

chanical one are not independent one from the other but they interact with each other in an iterative way.

2.1 Mean Line Thermodynamic Analysis

The thermodynamic analysis is the one that leads the design of the machine.

The code is based on a direct problem approach. This means that, given the shape of a profile, it is possible to evaluate its performance with a zero dimensional correlative approach and the analysis of the turbine is made through a Mean Line Analysis.

The code selects a two-dimensional constant profile section blading that is the same for stator and rotor rows. In fact, owing to expanding flow in both stator and rotor in a typical 50 % reaction stage and to the low loading level, it is recognized that with a single efficient profile section it is possible to cover the entire application range without any significant loss in efficiency (Havakechian and Greim [8]).

This two-dimensional constant profile section blading features a wide incidence range and a good mechanical behaviour. We can indicate this profile as "GEO-1".
The code knows the optimum conditions at which the profile presents its best efficiency point (BEP) in terms of:

- Flow Coefficient φ
- Stagger Angle ξ

Through an iterative approach, the code designs each single drum of the turbine with stages working at their BEP. When this is not possible, due to constraints in terms of maximum drum length or design diameters, the code is allowed to explore other working points varying the blade stagger angle.

The code requires only few inputs:

- Steam inlet conditions in terms of pressure and enthalpy
- Drum inlet and outlet hub diameters
- Discharge pressure

With these few inputs the code realizes a very first design of the drum in terms of:

- Number of stages
- Stagger angle of each stage ξ
- Flow coefficient φ
- Load Coefficient ψ
- Heights of blades

This first design is obtained knowing the $\varphi - \psi$ curves of the profile for each stagger angle. At the first iteration the drum efficiency is an hypothesis and only with the subsequent iterations this value is updated until convergence.

A schematic flow chart is reported in Fig. 2.2.

Into the code the row efficiency is calculated through a correlative approach coupled with a mean line analysis.

Once the first design of the turbine is performed the code starts the mechanical verifications.

2.2 Mechanical Verifications

Once the turbine structure is defined on the base of the thermodynamic analysis, the code performs a mechanical verification of the bladings (stator and rotor ones) and of the rotor anchor system.

This analysis leads to the dimensioning of the stator and rotor blade chord. The chord is dimensioned at first targeting an ideal aspect ratio value AR (blade height/blade chord).

The blade is modelled as a fixed beam and the most stressed section is verified. The chord is increased until the mechanical verifications are passed.

Furthermore, it is designed the foot of the rotor blade (its anchor system) and it is verified the resistance in terms of compression and bending.

The thermodynamic analysis and the mechanical verifications are not parts separated into the code. In fact, once the mechanical design is performed, a new thermodynamic analysis is carried out.

An iterative design procedure is hence realized until the turbine's performance between two subsequent steps is not varying (with respect to a minimum tolerance value).

At the end, it is verified that the calculated axial length is not greater then the maximum allowable one. When this happens, the code re-starts the design from the beginning with a reduced number of stages. A schematic flow chart is reported in Fig. 2.3

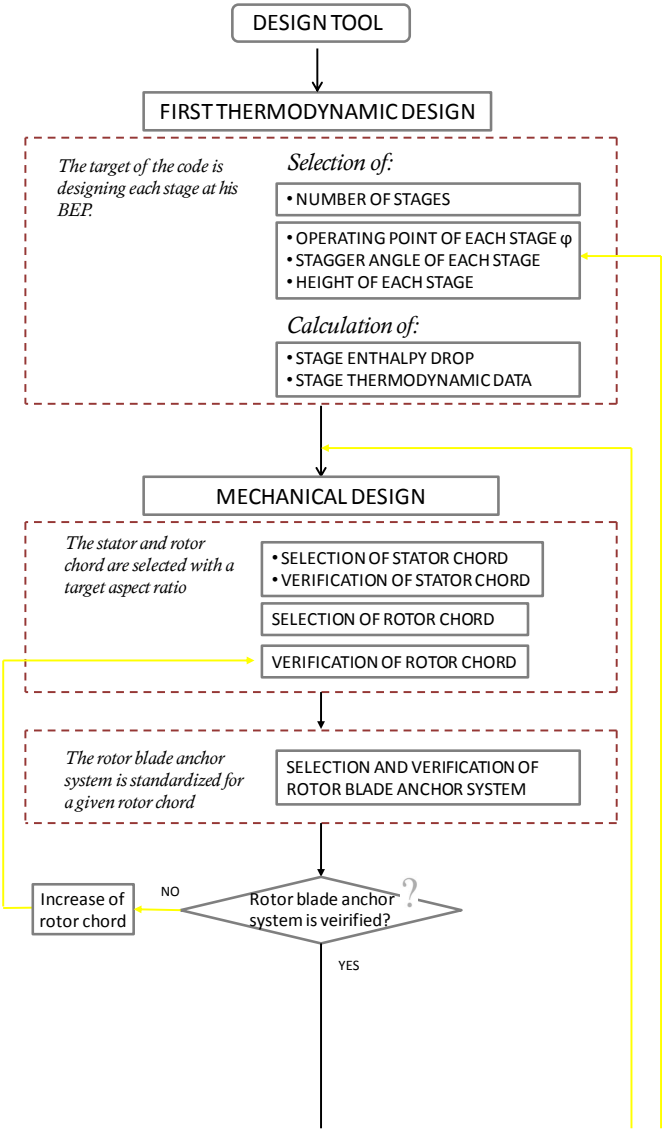
DESIGN TOOL
FIRST THERMODYNAMIC DESIGN
The target of the code is designing each stage at his BEP.
Selection of:
• NUMBER OF STAGES
• OPERATING POINT OF EACH STAGE φ
• STAGGER ANGLE OF EACH STAGE
• HEIGHT OF EACH STAGE
Calculation of:
• STAGE ENTHALPY DROP
• STAGE THERMODYNAMIC DATA
MECHANICAL DESIGN
The stator and rotor chord are selected with a target aspect ratio
• SELECTION OF STATOR CHORD
• VERIFICATION OF STATOR CHORD
SELECTION OF ROTOR CHORD
VERIFICATION OF ROTOR CHORD
The rotor blade anchor system is standardized for a given rotor chord
SELECTION AND VERIFICATION OF ROTOR BLADE ANCHOR SYSTEM
Rotor blade anchor system is veirified?
NO
Increase of rotor chord
YES

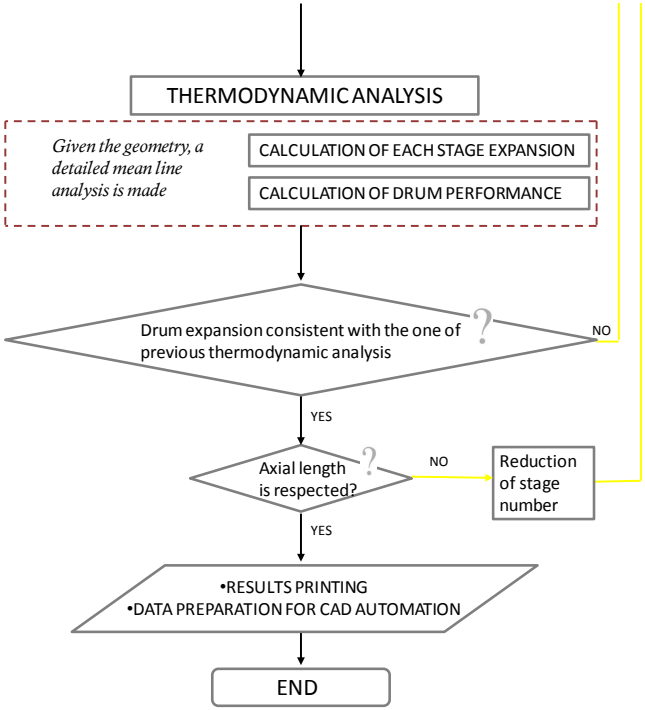

Figure 2.1: Code Schematic Flowchart

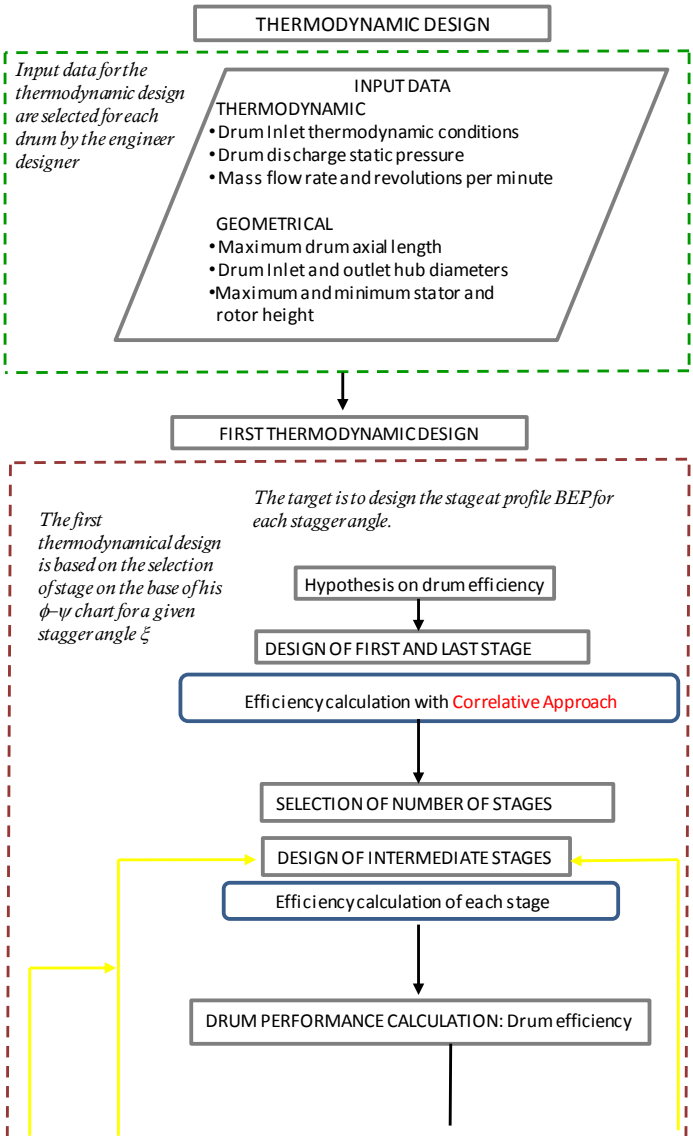
THERMODYNAMIC DESIGN
Input data for the thermodynamic design are selected for each drum by the engineer designer
INPUT DATA
THERMODYNAMIC
• Drum Inlet thermodynamic conditions
• Drum discharge static pressure
• Mass flow rate and revolutions per minute
GEOMETRICAL
• Maximum drum axial length
• Drum Inlet and outlet hub diameters
• Maximum and minimum stator and rotor height
FIRST THERMODYNAMIC DESIGN
The first thermodynamical design is based on the selection of stage on the base of his ϕ–ψ chart for a given stagger angle ξ
The target is to design the stage at profile BEP for each stagger angle.
Hypothesis on drum efficiency
DESIGN OF FIRST AND LAST STAGE
Efficiency calculation with Correlative Approach
SELECTION OF NUMBER OF STAGES
DESIGN OF INTERMEDIATE STAGES
Efficiency calculation of each stage
DRUM PERFORMANCE CALCULATION: Drum efficiency

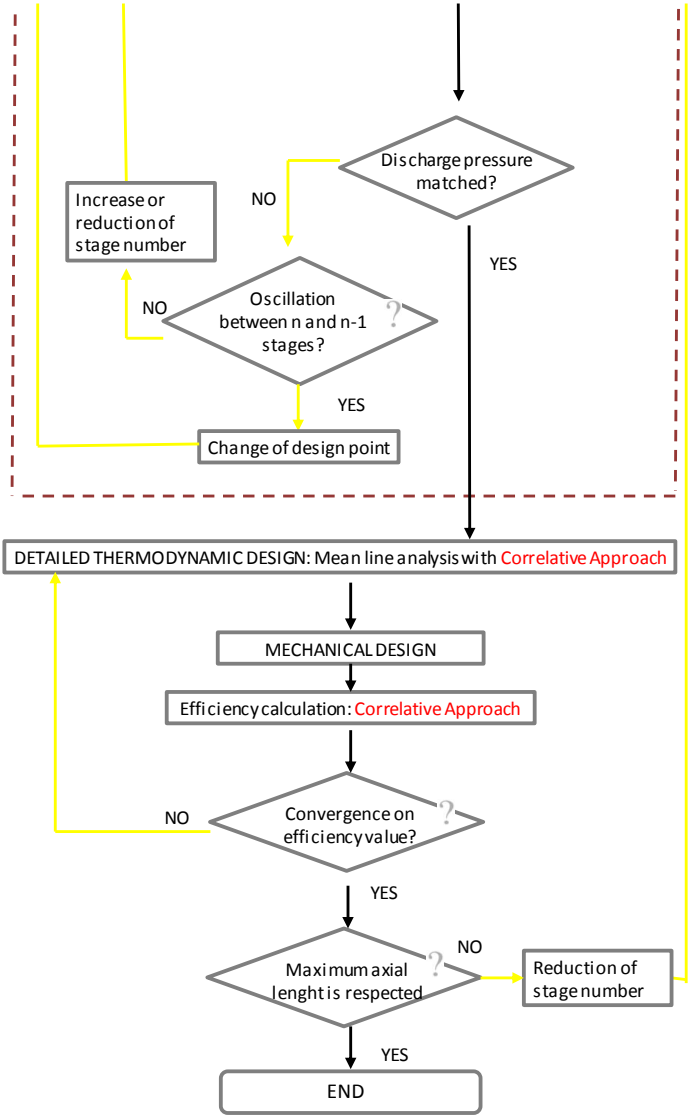

Figure 2.2: Thermodynamic design Flowchart

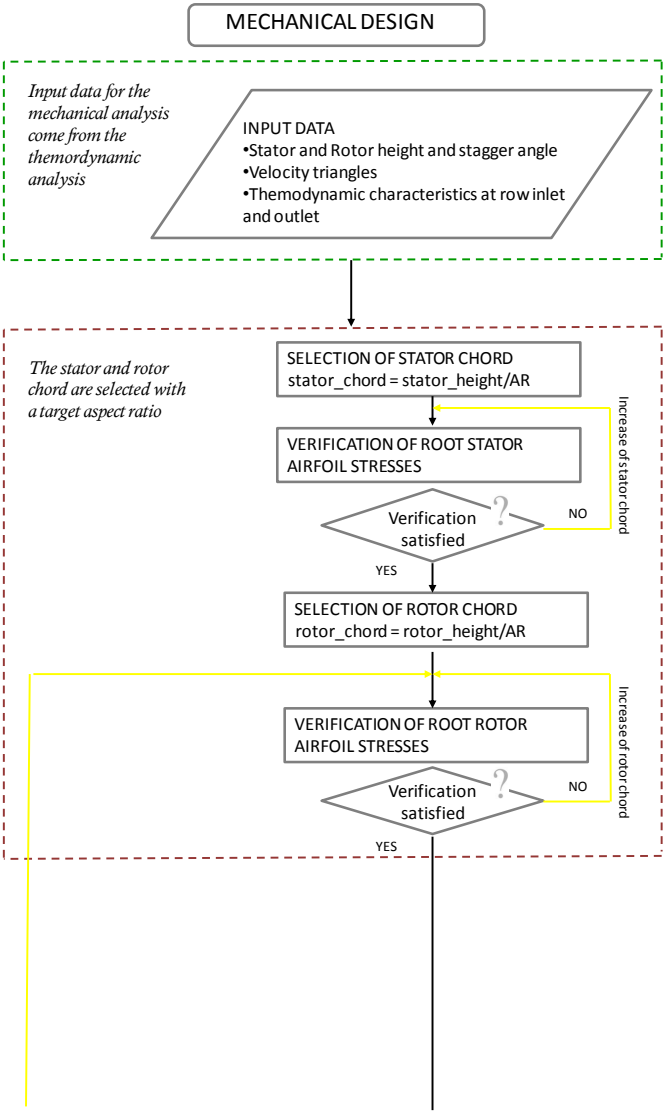
MECHANICAL DESIGN
Input data for the mechanical analysis come from the themordynamic analysis
INPUT DATA
•Stator and Rotor height and stagger angle
•Velocity triangles
•Themodynamic characteristics at row inlet and outlet
The stator and rotor chord are selected with a target aspect ratio
SELECTION OF STATOR CHORD
stator_chord = stator_height/AR
VERIFICATION OF ROOT STATOR AIRFOIL STRESSES
Verification satisfied
NO
YES
Increase of stator chord
SELECTION OF ROTOR CHORD
rotor_chord = rotor_height/AR
VERIFICATION OF ROOT ROTOR AIRFOIL STRESSES
Verification satisfied
NO
YES
Increase of rotor chord

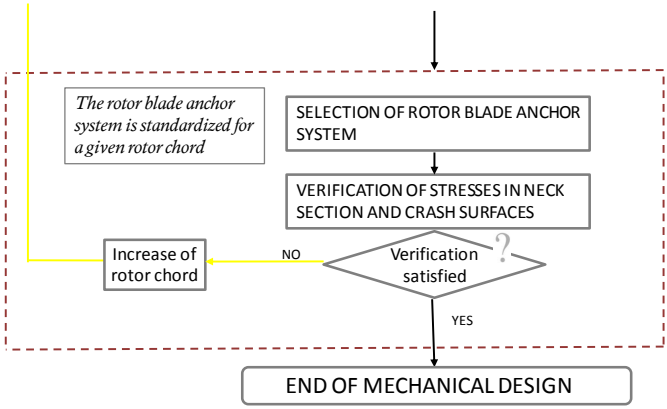

Figure 2.3: Mechanical design Flowchart

Chapter 3

Research of Efficiency Increase

This chapter provides a description of how the research of efficiency increase has been pursued

The 50 per cent reaction turbine stage (reaction stage) has often been synonymous with stages of superior aero-dynamic efficiency and high flexibility with respect to operating range.

This advantage is primarily linked with the lower stage loading and accelerating flow through the stator and rotor. To achieve the highest efficiency level the designer has to:

1. use the most efficient **profile sections**
2. find the optimum choice of the basic design parameters leading to the most efficient **meridional flow path**
3. optimize the **seal design** in order to reduce leakage flow rate and the impact on main flow rate

In the present thesis it has been investigated the research of more efficient machines through the use of more efficient

profile sections and meridional flow path.

3.1 Profile Geometry

As we have seen in the previous chapter, the existing code uses a profile of a given shape to cover the entire operating range. The code has in fact the task to design a turbine where this profile works at his best efficiency point BEP.

The code performs an iterative loop and the target is the design of a turbine that realizes the disposal of the flow for a given pressure ratio at the highest efficiency reachable with the given bladings. Then the tool performs the mechanical verifications. Mechanical verifications and thermodynamic design are coupled and interact one with the other until "convergence "on both.

This design approach is motivated by the fact that in the Steam Turbine world, especially the one of mechanical driven, the integration of the mechanical and thermodynamic design is really important, by the moment that the turbine has to be designed on the customer requirements.

Furthermore, in the case of Nuovo Pignone-GE Oil&Gas world, it is applied the design concept of "building blocks ", that are used to "assemble "the machine, that implies a very high degree of standardization.

Hence, when we have faced the problem of increasing profile efficiency, we have analysed two different possible paths:

1. Implementation into the code of a new more efficient profile geometry

2. Change of the design process with the introduction of a dedicated profile design section (i.e. resolution of meridional and blade to blade flow field, Havakechian and Greim [8])

The second way meant a complete change in the design procedure, and was not consistent with the requirements in terms of customization possibilities by a side (very variable customer's requirements) and standardization of product development process by the other.

Even if this way has the advantage of allowing the selection of the best profile section for each operating condition, industrial needs typical of this turbomachinery's field made not viable this approach.

It has been hence decided, together with the industrial partner, to find a new more efficient profile, so on called "GEO-2", to be used in alternative to the old profile GEO-1.

When looking for a new profile geometry, it was possible to follow two paths:

- Choice of a New prismatic (2D) profile
- Choice of a New three-dimensional blading design

During the last decade, the major steam turbine manufacturers have devoted significant investment on advanced three-dimensional blading design.
At the same time through the latest generation of two-dimensional constant profile section blading it has been recorded a reliable operation and outstanding performance in the entire range of setting angle , aspect ratio AR and stage loading ψ (Havakechian and Greim [8]).

Together with the industrial partner, it has been chosen to follow a more conservative path with respect to what it is actually implemented and to find an optimized new prismatic profile.

In fact, the adoption of a 3D profile would have implied a complete review of the mechanical verification approach and at the same time a strong effort in all the subsequent

phases of product development process, especially in terms of manufacturing.

Only at a later time of the present industrial research program it will be explored the opportunity of implementing a new more efficient three-dimensional blading design.

The new prismatic profile has been obtained through a dedicated multi-objective, aerodynamic optimization that relies on a neural-network based approach coupled with CFD analysis (Bellucci et al. [5]).

3.1.1 Airfoil Optimization

The overall optimization strategy is extensively reported in (Bellucci et al. [5]). Even if this optimization is not part of the present thesis, it is important to present here how this optimization has been performed.
This optimization relies on a neural-network-based approach and consists of coupling CFD analyses with a neural-network-based-optimization method. The CFD calculation have been performed by means of the multi-row, multi-block version of the TRAF code (Arnone [2], Arnone [3]).

Two different optimizations have been carried out, at high and low flow coefficient φ, by the moment that the optimized stage will work in a wide range of operating conditions.

By the moment that accounting for structural limitations was essential for final design purpose, both the static and dynamic behaviors of each geometry were checked downstream of CFD analysis.

The mechanical integrity checks are based on simplified design rules based on the evaluation of:

- Root Tensile Stress σ
- Minimum inertia moment-to-area ratio

Respecting the design philosophy of the tool, a single airfoil for stator and rotor rows was used. As a result of the

process two different optimum airfoils were identified:

- OPT-A: low φ
- OPT-B: high φ

and each one of these airfoils were tested in off-design conditions by varying the stage pressure drop. In addition both optimized airfoils were re-staggered to cover the whole operating range.

Hence, the profile optimized for high flow coefficient has been tested at low flow coefficient and vice versa.

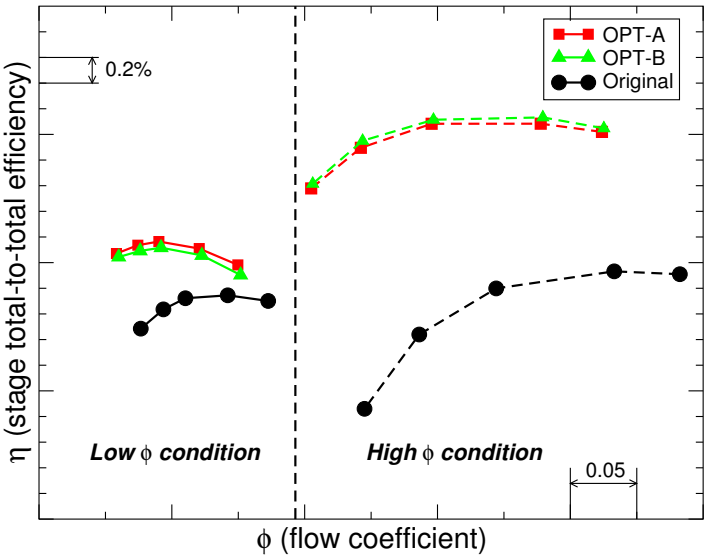

Figure 3.1: Efficiency comparison: original and optimized geometries performance curve (CFD)

Fig. 3.1 shows the comparison between the efficiency curves of the original airfoil (GEO-1) and those of the optimized airfoils (OPT-A and OPT2). The new geometries exhibit similar

operating range as the original and maintain an elevated efficiency gain in off-design conditions. Fig.3.1 shows also how the performance of the OPT-A is similar to the re-staggered version of OPT-B and vice versa.

The mechanical constraints, independent of the operating conditions, have driven the two optimizations towards similar airfoils shapes.

This has suggested the possibility of using a single optimized airfoil. The OPT-A was hence selected to cover, by re-staggering, the entire operating range. From this moment on we will refer to this optimized profile as GEO-2.

Compared to the original design, the GEO-2 geometry has a higher nominal stagger angle, a smaller radius of curvature in the rear part of the suction surface and it is in general thinner [Fig. 3.2].

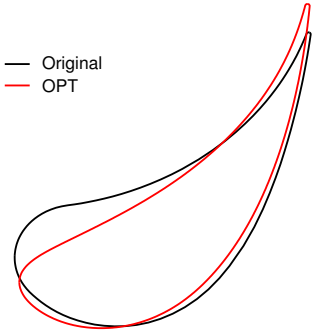

Figure 3.2: Airfoil geometries comparison(GEO-1 Original and GEO-2 Optimized

Parallel to the numerical activity, an experimental campaign was conducted in which the original GEO-1 and GEO-2 airfoils were tested in a linear cascade arrangement. A general agreement was found between measurements and predictions in terms of shape of the loss coefficient curves. Moreover the loss level was fairly well predicted too, since the maximum er-

ror between computations and measurements was lower then 0.3%.

3.1.2 Implementation in the design procedure: Thermo-fluid dynamic analysis

By the moment that the existing design tool performs both a thermodynamic as well as a mechanical strength analysis, it has been necessary to implement the new optimized geometry with respect to both aspects.

Concerning the first aspect, as aforementioned in chapter 2, the code performs a thermo-fluid dynamic analysis its scope is the calculation of:

- Row Efficiency
- Stage Enthalpy drop

Into the code this scope is realized using a zero-dimensional correlative approach together with a mean line analysis. When facing the problem of introducing the new profile GEO-2 into the code by a thermodynamic point of view few alternative approaches have been taken in consideration.

The constraints to the problem were:

- The new approach has to be easily integrated into the existing code
- The new approach must require a computational time compatible with the existing design cycle time

The approaches that have been taken in consideration are:

1. A zero dimensional correlative approach coupled with a Mean Line Analysis
2. A zero dimensional correlative approach coupled with an analysis of the flow field outside of the bladings with a Not Isentropic Radial Equilibrium (NISRE).

3. Solution of the three-dimensional flow field based on the resolution of meridional (S2) and blade to blade (S1) flow (Wu and Brown [14] and Havakechian and Greim [8])

The first approach is analogous to what is at the moment into the code, while the second approach would have allowed a better characterization of profile losses.

The last approach has been excluded by the industrial partner because of too tight time deliverable of the present research project.

Together with the industrial partner, we have decided to investigate the first approach, and, when not satisfying, to take in consideration the second one.

This decision has been supported by the consideration that the new profile geometry is a prismatic blade, hence the metal blade inlet and outlet angles remain constant along the span. On the other hand, the inlet flow angle varies with the radius ratio, but the new profile geometry, as well as the old one, is tolerant to incidence. Hence one can reasonably expect to have not a strong variation of profile loss along span.

An extensive CFD campaign has been carried out in order to investigate the effects of basic two-dimensional loss, secondary flow and tip clearance on the stage efficiency.

In fact, by the moment that the goal was to replace the current set of correlations for the row performance estimations, the CFD campaign has been aimed at pointing out the differences in the aerodynamic behavior between two high-pressure steam turbine stages implementing respectively the GEO-1 and GEO-2 profile.

In order to find the best suitable correlative approach for the new blading, it has been deeply analyzed the one present into the code for the old (GEO-1) blading.

The last step has been the analysis of what is available in the open literature. At the end, it has been possible finding a new correlative approach that suits GEO-2 bladings.

CFD Campaign

Three dimensional RANS Analysis have been carried out in order to independently investigate the effect of profile, secondary flow and tip-clearance losses on the stage efficiency.

Fig. 3.3 shows a comparison between GEO-1 and GEO-2.

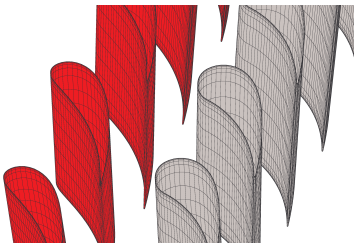

Figure 3.3: Three dimensional blade geometry comparison GEO-1 (black) and GEO-2 (red)

Both airfoils exhibit a blunt leading edge, in order to have a good robustness with respect to incidence, suitable for wide operating range where these blades typically operate. The geometrical differences in this region yield a different response to incidence variation, that plays an important role in affecting stage performance.

The higher nominal stagger and the smaller radius of curvature of the uncovered part of the suction side of GEO-2 respect to GEO-1, together with higher pitch-to-axial chord ratio, provide an increase in the blade loading.

An exhaustive comparison between the performance of the two geometries was then carried out. The parametric study included geometrical features such as:

- Stagger angle ξ
- Aspect ratio AR
- Radius ratio RR

This study was extended in a wide range of flow coefficient (ϕ) in order to cover the expected operating space. A cylindrical flow path geometry was selected to avoid local three-dimensional effects that can hide the actual impact of the parameter under investigation. For each configuration, a performance curve was drawn by varying the stage backpressure only, while keeping the same pressure and temperature distribution at stage inlet.

Impact of Profile losses The impact of the profile loss on the efficiency of the two stages was studied by varying the stagger angle of the blade. In fact, by the moment that both stages GEO-1 and GEO-2 employ prismatic blades, use a single airfoil for stator and rotor rows and are designed to work with an optimum pitch-to-chord ratio at blade midspan, the only geometrical feature that can affect profile loss, with a fixed blade size and flow path geometry, is the stagger angle.

The computations were performed in a cylindrical flow path characterized by a high AR and low RR, in order to limit the influence region of the secondary flows near the endwall. Hence the evaluation of the midspan loss was not affected by secondary flows. The results of this analysis are reported in Fig. 3.4

The Fig. 3.4 highlights that the envelope curve of the peak efficiency for the GEO-2 has a greater efficiency. The total loss coefficient ζ was evaluated making a balance between the inlet and the outlet section of the computational domain, while the profile loss was calculated at the blade midspan. Both are evaluated with the equation 3.2:

$$\zeta = 1 - (\frac{c_2}{c_{2is}})^2 \tag{3.1}$$

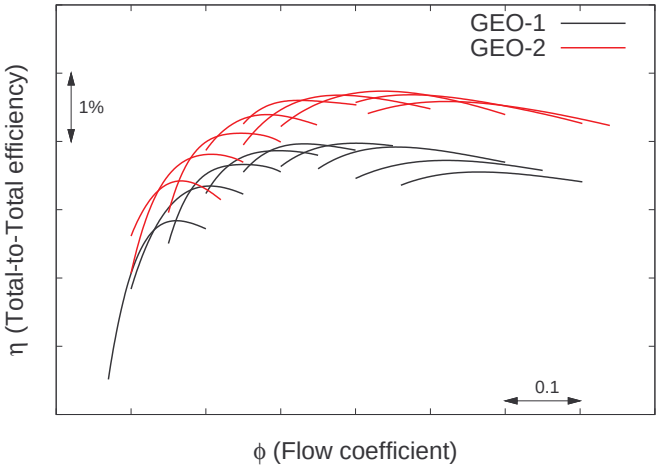

Figure 3.4: Comparison between GEO-1 and GEO-2 performance curves at different stagger angles

and:

$$\zeta_{sec} = \zeta_{tot} - \zeta_p \tag{3.2}$$

The trends of the loss coefficients are reported in Fig. 3.5.

Observing the profile losses, it is worth noticing that the benefits of the GEO-2 rise towards the reduced staggers. This consideration highlights that only the aerodynamic performance of the airfoils guides the $\Delta\eta$, revealing that both stages have a similar behavior in terms of secondary flows. The Fig. 3.5 shows how the impact of secondary loss is almost constant in the whole range.

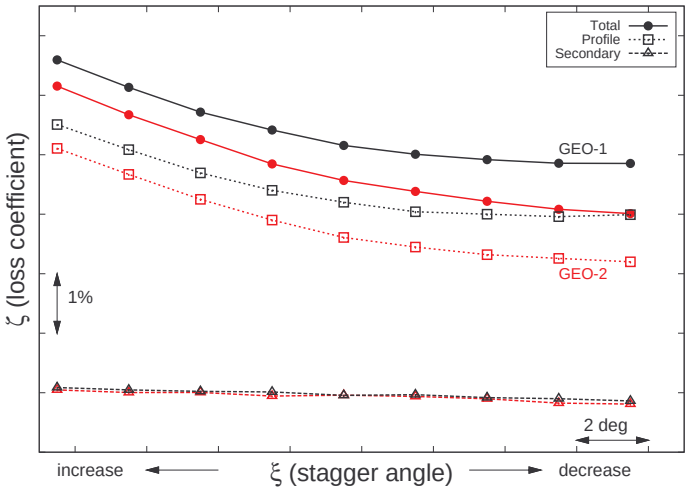

Figure 3.5: Total, profile and secondary loss coefficients at different stagger angles: comparison between GEO-1 and GEO-2 (constant AR,RR,Reynolds Number)

Impact of Secondary losses The effects of secondary flows were studied at three different stagger angles, by varying independently the blade aspect ratio AR and radius ratio RR of the meridional flow path. At first the impact of Aspect Ratio was investigated at four different values. The blade height was varied at fixed chord length in order to preserve the same Reynolds number. For each AR a flow path geometry with different mean diameter was selected in order to keep the radius ratio unchanged. Moreover the blade speed was modified to preserve the kinematic similitude of the stage at midspan.
The results of the computations are reported in Fig. 3.6 where the peak efficiency is reported for both stages at three different stagger angles. The computations confirm the well known trend whereby reducing AR increases the blade span influ-

enced by the secondary flows, thus reducing efficiency.

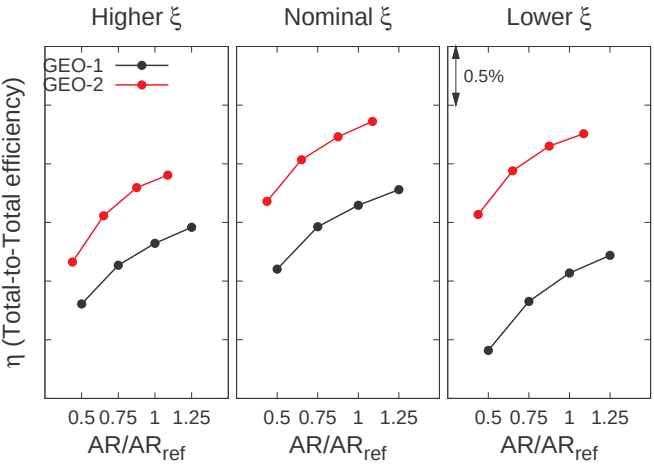

Figure 3.6: Aspect ratio effect for three values of stagger angle: comparison in terms of peak efficiency values

The two stages exhibit similar secondary flows intensity and depth of penetration into the main stream, as shown in Fig. 3.7. The figure shows how the secondary flows increase their penetration with reduced AR and higher stagger angles, affecting the aerodynamic performance of the stage. The percent of the blade height influenced by these flows is almost the same for both stages.

As for the aspect ratio analysis, four different values of Radius Ratio were investigated. The computations were performed with different flow path geometries and blade speeds in order to preserve the Aspect Ratio and the kinematic similitude of the stage at midspan for each RR. The results are summarized in Fig. 3.9. Increasing the radius ratio increases the variation of inlet flow angle. The endwall regions work in

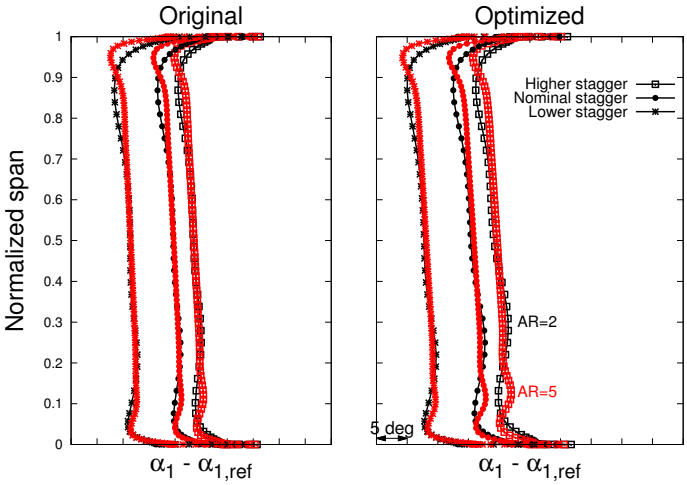

Figure 3.7: Aspect ratio effect: spanwise distribution of swirl angles at bucket exit for several stagger angles

very off-design conditions. For these reasons the efficiency is progressively reduced when the radius ratio is increased, as shown in Fig. 3.8.

When comparing the two stages, a similar angle distribution can be observed for the lower radius ratio, as well as the same penetration of the secondary flows in the mainstream. Different considerations have to be made for the $RR/RR_{ref} = 1.33$ case. The impact of secondary flows is stronger for GEO-2 stage and more marked for the higher stagger.

Choice of correlative approach

Most of the actual turbines selected currently by the design tool are composed of stages with high aspect ratios and low radius ratios, which confine three dimensional effects near blade endwalls. The discussion of the CFD results has pointed

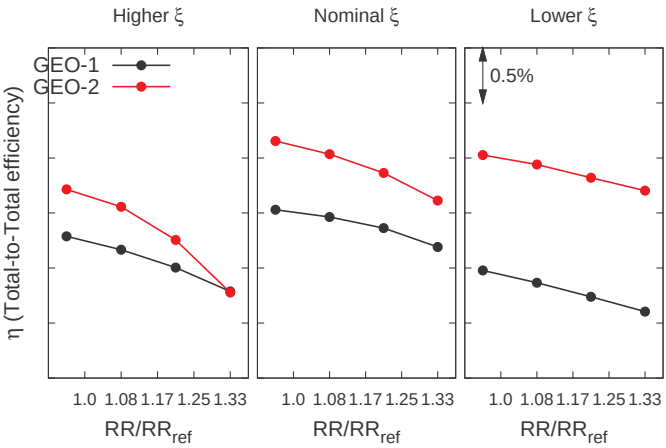

Figure 3.8: Radius ratio effect for three values of stagger angle: comparison in terms of peak efficiency values

out that the GEO-2 stage would have responded in a very similar way to the GEO-1 one in terms of secondary losses. Thus it was decided to use the **same modelling of the secondary losses as the one implemented in the existing correlations**. Once the model for secondary losses was established, the tuning was focused on the modeling of the profile loss.

At first we have analysed the current set of correlations implemented for GEO-2.
The correlative approach present into the code is based on the one of Traupel (Traupel [13]) with few modifications. Traupel has developed a one-dimensional, empirical model where various flow disturbances are generated by the presence of the blades. Extensive testing has been the base for empirical diagrams, and then these experimental results are interpreted

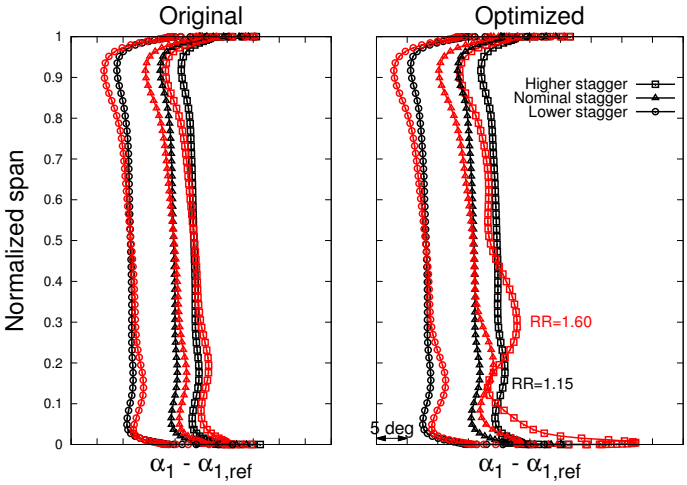

Figure 3.9: Radius ratio effect: spanwise distribution of swirl angles at bucket exit for several stagger angles

in a physical sense to be interpolated-extrapolated also for other flow and geometrical conditions. The total loss by Traupel consists of profile losses, secondary losses (rest losses), tip leakage losses and fan losses:

$$\zeta = \zeta_p + \zeta_f + \zeta_r + \zeta_{TIP} \tag{3.3}$$

where ζ is defined as:

$$\zeta = \frac{C_{2is}^2 - C_2^2}{C_{2is}^2} \tag{3.4}$$

The profile losses are due to the friction on the profile surfaces and the separation of the boundary layer on the blade. The profile losses ca be calculated as:

$$\zeta_p = \chi_R \chi_M \zeta_{p0} + \zeta_{TE} + \zeta_c \tag{3.5}$$

- ζ_{p0}: the basic profile loss is a function of outlet flow angle.

- χ_R: Reynolds number correction. A high Reynolds number (above 2×10^5) has no effect on the profile loss, while a low Reynolds number will increase the profile loss. The surface roughness has a large impact on Reynolds number correction factor and its influence can be seen for value of roughness-to-chord ratio above 10^{-05}.

- χ_M: The Mach number correction takes into account what impact the outlet Mach number has on the profile loss.

- ζ_{TE}: The trailing edge loss depends on the trailing edge thickness to pitch ratio, basic profile loss, Mach and Reynolds number correction. For steam turbine blades, where the TE thickness tipically is small, this loss has little influence.

- ζ_C: The Carnot shock loss is caused by the shock that appears just after the TE where the fluid undergoes a sudden expansion. For steam turbines this loss is typically predominated by the flow angles at given TE thickness.

As it can be seen, the old set of correlations made a point only of the **outlet flow angle**. Some geometrical features of the blades were also implicitly assumed, such as the deflection or the maximum blade thickness. For these reasons, a more general profile loss model was necessary, capable of reproducing the correct trend of incidence losses and including a more exhaustive set of input parameters.

Many loss predictions methods exist to predict losses in turbomachines. Concerning axial turbines, methods for predicting total losses in the cascades have been developed such as:

- Ainley & Mathieson -[1951] [1]
- Craig & Cox -1970 [7]
- Duhnam & Came [1970]
- Traupel -1977 [13]
- Kacker & Okapuu - [1982] [9]
- Moustapha & al -[1990] [10]
- Benner & al -[1990] [6]
- Aungier -2006 [4]

All these approaches handle the impact of incidence on the profile loss. In general, the loss is calculated at design condition and then corrected for the off-design ones as a function of the incidence angle. The differences among these works have to be sought not only in the parameters used to describe the airfoil geometry, but also in the complexity of the models themselves. This makes each approach effective and accurate for a specific blade typology, somehow losing its prediction capability when different typologies are faced.
In light of this consideration, each approach has been examined in depth, and eventually it has been defined a proper blending of such approaches, in order to exploit the advantages of each for the case under investigation.
Much attention was paid to the leading edge geometry of the profile, which is markedly different between GEO-1 and GEO-2. In fact, the characterization of the leading edge is recognized in literature as a key factor in estimating profile performance (Moustapha et al. [10] and Benner et al.[6]), as it plays a role of primary importance in determining the incidence losses. The input parameters were extended, including some geometrical features such as the blade thickness, inlet flow and blade angle as well as the outlet ones and the leading edge diameter. However, all the details of such a "blended" are

proprietary and cannot be disclosed in the present thesis.

A first validation of the new set of correlations was made by considering the cylindrical flow path geometry used to investigate the impact of profile loss. The prediction of the new correlations were compared with the ones by the old set and CFD results at different stagger angles.
The results are summarized in figures 3.10 and 3.11, where the performance curves of the GEO-2 stage are evaluated by means of the three tools: CFD calculation, Old Correlative Set, New Correlative Set. A general agreement was found between CFD and the tuned correlations. When comparing the two figures, the need for tuning the 1-D tool to correctly model the GEO-2 stage into present design tool is readily evident. The tuning has allowed for a better prediction not only in terms of absolute value, but also in terms of peak-efficiency and off-design behavior. For all the curves, except for the lower left one, the prediction is improved. This is probably due to the secondary loss model, which might not be able to accurately capture the impact of secondary flows for the GEO-2 geometry. In fact, to work along that working line, the blades had to have a high stagger angle, which enhances the secondary flows. However, the region where the tuning worsen the prediction capability is far from the optimum design space where the blades are commonly designed. Moreover, the difference in efficiency evaluation, between the old and the new curve, is about 0.25%. Overall, the trend of each curve and the shape of the envelope curve confirm the interpretation of the CFD results discussed in the previous section.

In order to assess the prediction capability of the new set of correlations in different machine layouts, than the one used for the tuning, two different stage configurations were extracted from existing turbines. These two geometries are characterized by different meridional flow paths (AR,RR), ro-

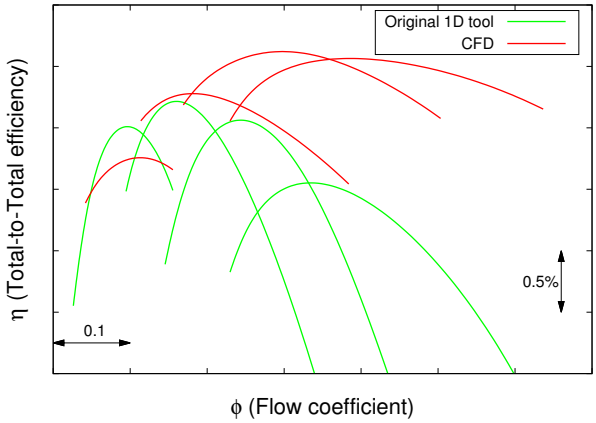

Figure 3.10: Original 1D tool: stage performance prediction

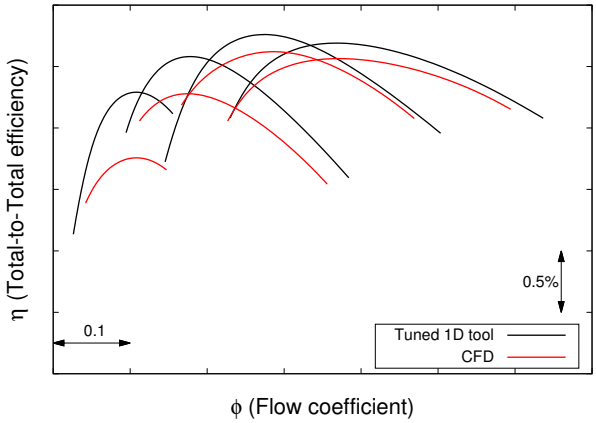

Figure 3.11: Tuned 1D tool: stage performance prediction

tational speeds, expansion ratios, flow coefficients and blade counts. The GEO-2 airfoil was investigated in design and off-design conditions by means of CFD computations. The results were compared to the one-dimensional prediction tool as depicted in Fig. 3.12. The plots show a general good agreement between CFD and the preliminary design tool in terms of both peak efficiency position and absolute value. The tuned tool predicts an off-design behaviour similar to the one of CFD computations, highlighting that the new modelling is able to well capture the aerodynamic behavior of both the stages. Moreover, the results confirm the choice of using old modelling for the secondary losses.

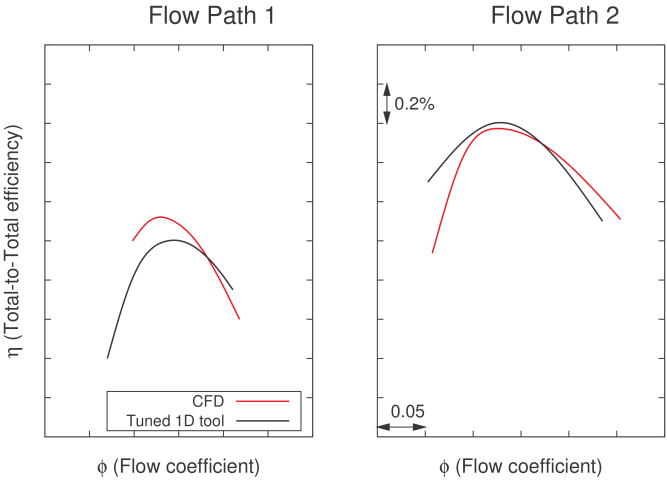

Figure 3.12: Performance curve for two different real machine layouts: comparison between CFD and tuned 1D tool

3.1.3 Implementation in the design procedure: Mechanical verifications

Once the thermofluiddynamic design is realized, the code performs mechanical and aero-mechanical verifications. Into the present work only the mechanical verifications have been revised and updated. First, it has been deeply analysed how the mechanical verifications are performed into the code, then, in light of some considerations, these have been revised and updated.

The design procedure presents an high grade of standardization. This means that, even if the code designs turbine in a wide operating range, the parts of the machine itself are deeply standardized.

In particular the design basic element is the blade chord. Once the blade chord is defined, all the other parts, for instance the cover or the anchorage system, are dimensioned as a function of this one.

The mechanical design starts with the dimensioning of the stator and rotor chord. Once the chords are verified, it is possible to design the other components and make the relative mechanical verifications. If one of the verifications related to these component is not satisfied, we go back to the chord dimensioning that is increased until all the verifications are passed.

Existing Mechanical verifications into the code

The mechanical verifications into the code are performed assuming the stator and rotor blade like a fixed beam. Furthermore also the rotor anchor system, the "blade foot", is verified.

The stator and rotor chord are selected considering a target aspect ratio. The value of this target aspect ratio depends

on many factors, for instance if we are considering the first stage or a subsequent one or the value of steam quality.

The chord is hence calculated as:

$$chord = \frac{H_{blade}}{AR} \tag{3.6}$$

Once the stator chord and the rotor chord are verified, the rotor anchor system is verified too. The chord is increased every time one of these verifications is not passed, until a maximum value.

Blade mechanical verification The schema of the blade mechanical verifications is reported in Fig. 3.14. The blade is verified in its root section. The blade is modelled like a fixed beam. Both static and fatigue stress are calculated only in one point of the airfoil contour. This is due to two reasons:

- The point of the airfoil contour where the stress is calculated is in most cases the most stressed one
- At the time when the program has been written it was essential saving computational time.

We can indicate this point as "point A". The turbine's blade can be considered well dimensioned when:

- The total static stress is lower then an allowable value calculated for a static load
- The bending stress is lower then the alternate allowable stress

The **static stress** σ_{stat} is calculated considering:

1. Membrane stress due to centrifugal force acting on the blade cover σ_{c1}

$$\sigma_{c1} = \frac{Fc_{cover}}{A} \tag{3.7}$$

2. Membrane stress due to centrifugal force acting on the blade σ_{c2}

$$\sigma_{c2} = \frac{Fc_{blade}}{A} \tag{3.8}$$

3. Bending stress due to steam force σ_{b1} calculated in the point A

The total stress in point A is hence:

$$\sigma_{stat} = \sigma_{c1} + \sigma_{c2} + \sigma_{b1} \tag{3.9}$$

The **fatigue stress** is calculated considering:

1. Membrane stress due to centrifugal force acting on the blade cover σ_{c1}

2. Membrane stress due to centrifugal force acting on the blade σ_{c2}

3. Bending stress due to steam force σ_{b1} calculated in the point A

For each material, selected by the designer, the allowable stress is selected as a function of operating temperature.

The modelling of the blade cover is approximate. The contribute to stress due to the presence of the cover is taken into account only in terms of membrane stress and not in terms of bending. Even if the centrifugal force acting on cover creates a bending stress, due to the fact that its center of gravity is not aligned with the one of the blade root section, by the moment that this one is opposite respect to the steam one, it is not considered.

Rotor blade anchor system mechanical verification
The rotor blade anchor system is verified taking into account the stresses at:

Figure 3.13: Point A of the airfoil contour verified in mechanical analysis

- Foot neck section
- Crash surfaces

In this section the stresses considered are:

- Membrane stress due to centrifugal force acting on the blade cover σ_{c1}
- Membrane stress due to centrifugal force acting on the blade σ_{c2}
- Membrane stress due to centrifugal force acting on the foot σ_{c3}
- Bending stress due to steam force σ_{b1}
- Bending stress due to centrifugal force acting on the blade at foot neck section σ_{b2}
- Bending stress due to centrifugal force acting on the blade at crash surfaces section σ_{b22}

The steam force consists of two parts:

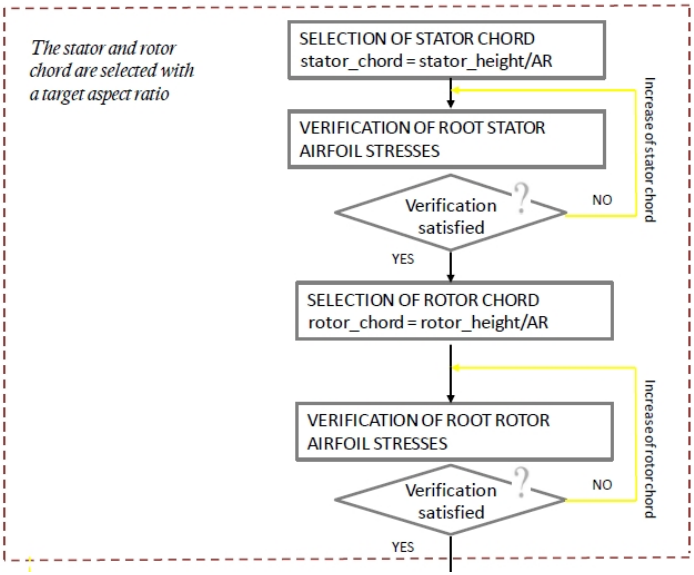

Figure 3.14: Stator and Rotor blade design flow chart

- pressure of steam acting on blade surface
- the change of steam momentum

Also the centrifugal force acting on cover and the upper part of the foot create a bending stress of foot neck and crash surfaces. In the existing coed they have been considered negligible.

Review and update of mechanical verifications into the code

First, in order to perform the mechanical verifications when the new profile geometry is selected, it has been necessary to update a series of geometrical parameters.

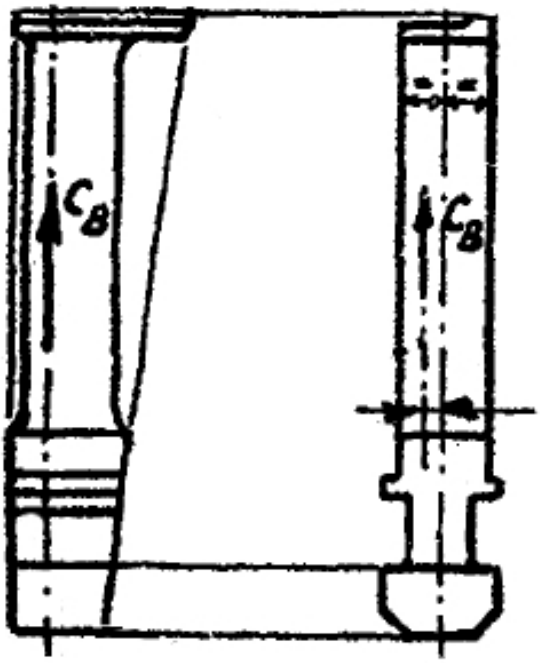

Figure 3.15: Blade centrifugal force

In particular, have been updated the values of:

- Minimum and maximum inertia moment in principal inertia reference system
- Airfoil area
- Airfoil coordinates in principal inertia reference system of the most stressed point of the airfoil.

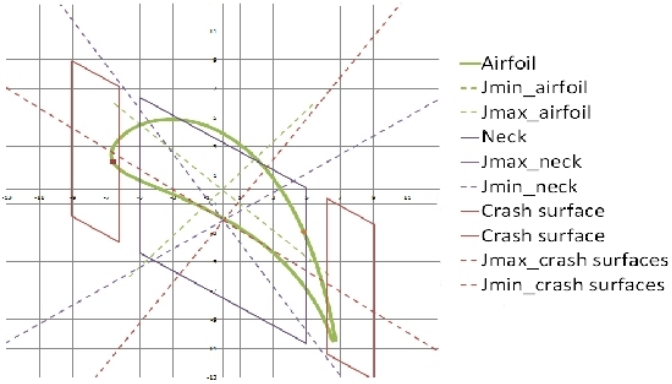

Figure 3.16: Inertia axis

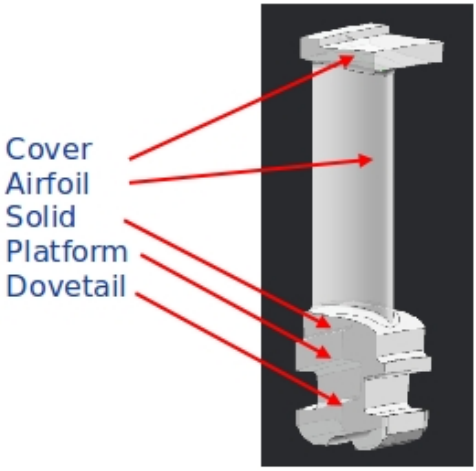

Figure 3.17: Rotor Blade

Considering that the computational cost is not anymore a critical factor, it has been decided to improve the accuracy of stress modeling.

At first it has been decided to extend the number of verifications at the root blade section. Hence it is verified not only one point but a discrete number of points that properly describes the airfoil shape. In the new version of the code the airfoil's shape is hence discretized in 47 points and they are all verified.

Improvement in foot geometry realised by the industrial partner have been implemented into the code, hence it has been implemented the new foot modeling. In order to calculate the stresses it has been necessary to calculate the inertia momentum of each critical section of the foot in his principal inertia reference system, as reported in Fig. (3.16).

In order to reach a deeper detail in stress modeling, it has been decided to carefully model both the cover and the foot geometry:

- Cover: It is calculated the mass and the center of gravity. This allows a proper calculation of the bending due to the centrifugal force that acts at blade root section and at foot neck and crash surfaces.

- Foot: It is calculated the mass and the center of gravity. This allows a proper calculation of the bending due to the centrifugal force that acts on foot neck and crash surfaces.

This accurate modeling has allowed us to calculate all the bending stresses acting at blade root section and at foot critical sections, in particular:

- Bending stress due to centrifugal force acting on the cover at blade root section σ_{b3}

- Bending stress due to centrifugal force acting on the cover at foot neck section σ_{b4}

- Bending stress due to centrifugal force acting on the cover at foot crash surface σ_{b5}
- Bending stress due to centrifugal force acting on the upper part of the foot at foot neck section σ_{b6}
- Bending stress due to centrifugal force acting on the upper part of the foot at foot crash surfaces σ_{b7}

Thank to this new approach, it has been possible having a better modeling of the stresses acting on the critical sections of the blade and of the blade anchor system.

3.1.4 Implementation in the design procedure: Positioning in tangential direction of the blade respect to cover and blade foot

When facing the problem of the tangential positioning of the rotor blade respect to cover and foot, the old design procedure performed a standard positioning. No consideration was made upon the consequences in terms of stress connected to a given positioning respect to another.

When we have faced the problem of using the old rules for tangential positioning or finding new ones, we have realised that the tangential positioning does not have only an impact on the geometry of the machine, but also on the stresses acting on the critical sections of foot and blade. This is due to the misalignment along radial direction of the center of gravity of cover, blade root section and foot critical sections in tangential direction.

As we have seen in section 3.1.3, the centrifugal stress acting on the cover determinates a bending stress on airfoil and foot critical sections, as well as the centrifugal stress acting on the blade determinates a bending stress on foot critical sections. Even if in lower measure, also the upper part of the foot, whose center of gravity is not aligned with the one of the foot critical sections, determinates a bending stress on these last ones.

As we have seen, these stresses are influenced by the reciprocate tangential position of each part of the rotor:

- Bending stress due to centrifugal force acting on the blade at foot neck section σ_{b2}
- Bending stress due to centrifugal force acting on the

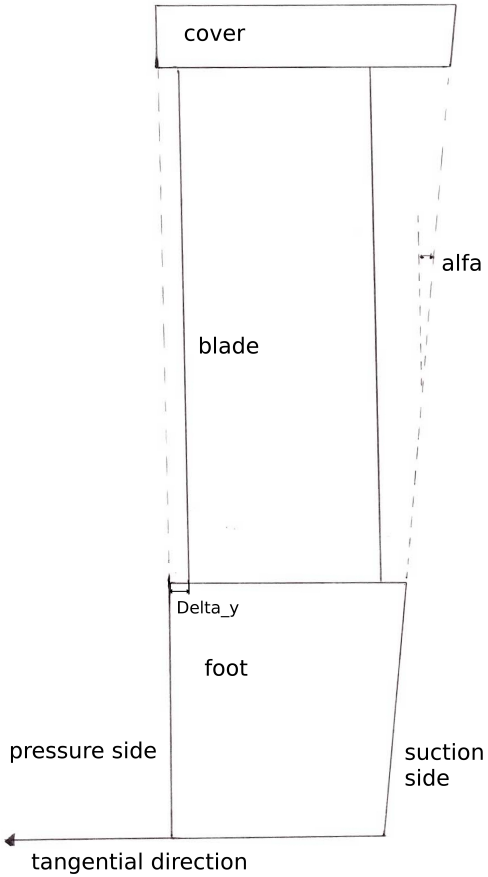

Figure 3.18: tangential view of the rotor

blade at crash surfaces σ_{b22}

- Bending stress due to centrifugal force acting on the cover at blade root section σ_{b3}

- Bending stress due to centrifugal force acting on the cover at foot neck section σ_{b4}
- Bending stress due to centrifugal force acting on the cover at foot crash surface σ_{b5}
- Bending stress due to centrifugal force acting on the upper part of the foot at foot neck section σ_{b6}
- Bending stress due to centrifugal force acting on the upper part of the foot at foot crash surfaces σ_{b7}

Obviously, only the component of the stress related to axial momentum is influenced by tangential positioning.

Research of optimum tangential positioning

By the moment that these stresses are influenced by the reciprocate tangential position of each part of the rotor, we have thought that it could be possible to **use this positioning to reduce the stresses acting on the critical sections**.

With reduced stresses it is possible to select a smaller rotor chord size. When, with the same operating conditions, it is possible to have a smaller chord the advantages are numerous.

In fact, what we expect from a reduced rotor chord size is:

- Increase in efficiency connected with an higher aspect ratio
- Reduced axial length. This is often connected with an increase in efficiency when the drum axial length is a strong constraint. In these cases in fact a reduced stage axial length means a higher number of stages working at lower load and closer to their best efficiency point.

The new rotor blades, respect to the old ones, will be manufactured with a **CNC machine with 5 axis**, hence we

have the possibility to explore the design space in terms of tangential positioning.

We have decided to set the relative positioning of blade, cover and foot with two parameters:

- alfa : angle of suction side respect to radial direction
- delta_y: distance in terms of tangential direction from blade pressure side to solid pressure side

In Fig.3.18 it is reported the basic configuration, with the pressure side of the blade aligned with radial direction and delta_y equal to its minimum value (there is a curvature radius that has to be respected between blade and solid).

Varying both these two parameters, alfa and delta_y, we can realize a matrix of possible configurations.

We have decided to **review the design procedure**, and in particular we have decided to make the verification of rotor and foot critical sections at the same time, and not in a sequential way, as it was in the code (see Fig. 2.3).

For each possible configuration in terms of alfa and delta_y, it is computed the ratio between acting stress and allowable one $\frac{\sigma}{\sigma_{all}}$ in each point of the critical sections .

We make hence a matrix its dimensions are:

- Number of positioning in terms of alfa
- Number of positioning in terms of delta_y
- Number of verifications

In Fig. 3.19 the matrix of possible design solutions is represented: at each couple of j-k value corresponds a geometry in terms of alfa and delta_y.

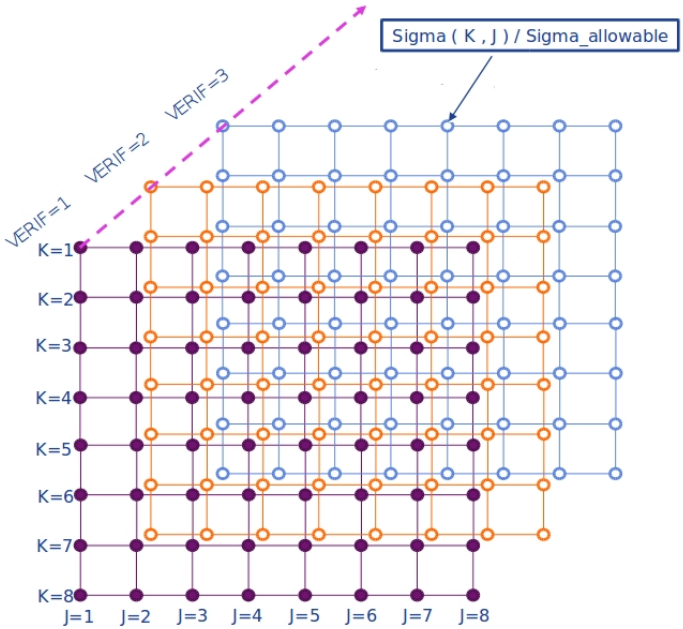

Figure 3.19: Design matrix

Once the matrix values are computed, it has been essential finding a criterion for the choice of the optimum configuration. The first criterion is obviously that the configuration to be chosen has to present all the $\frac{\sigma}{\sigma_{all}}$ values (corresponding to all the verifications) lower than 1.
In fig. 3.20 this means that only the configurations where all the curves are under the black line are taken in consideration.

Once these possible configurations have been found, we need a criterion for the choice of the best solution. We have taken into consideration two possible criteria:

1. Choice of the configuration with the minimum of the

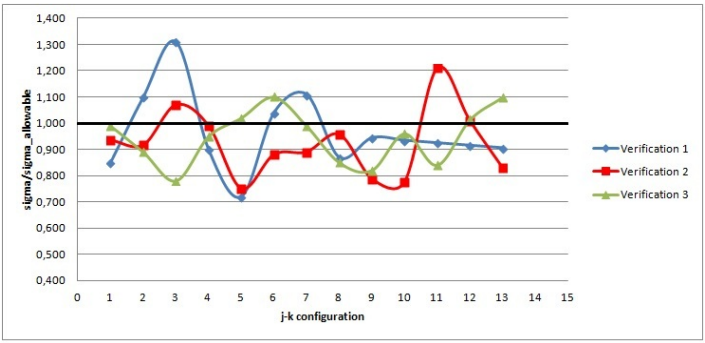

Figure 3.20: Example of Values of $\frac{\sigma}{\sigma_{all}}$

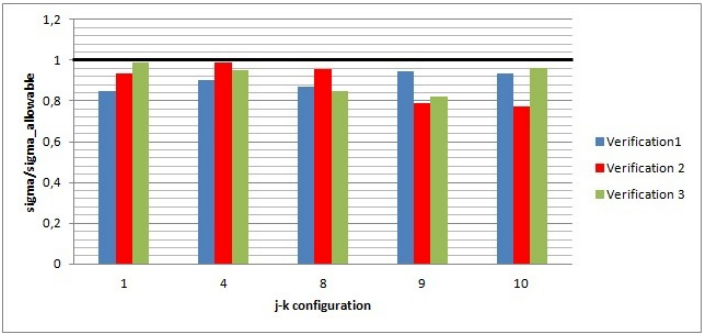

Figure 3.21: Example of Possible tangential configuration in terms of stresses

sum of the stresses:

$$\sigma_{tot} = \sum (\frac{\sigma}{\sigma_{all}}) \tag{3.10}$$

2. Choice of the configuration with the smallest "highest stress"

We have decided to choose the second one because this criterion leads to a better exploitation of the strength characteristics of the material in all the critical sections. We may say that the material is somehow "better used".

In Fig. 3.21 are reported the configurations where all the values $\frac{\sigma}{\sigma_{all}}$ are lower then 1. In the case reported in Fig. 3.21, on the base of the chosen criterion the selected configuration would be the **number 9**.

The new mechanical design procedure implemented into the code is reported in Fig. 3.22. As we can easily see now the selection of the blade rotor chord and anchor system is made at the same time and not with subsequent steps.

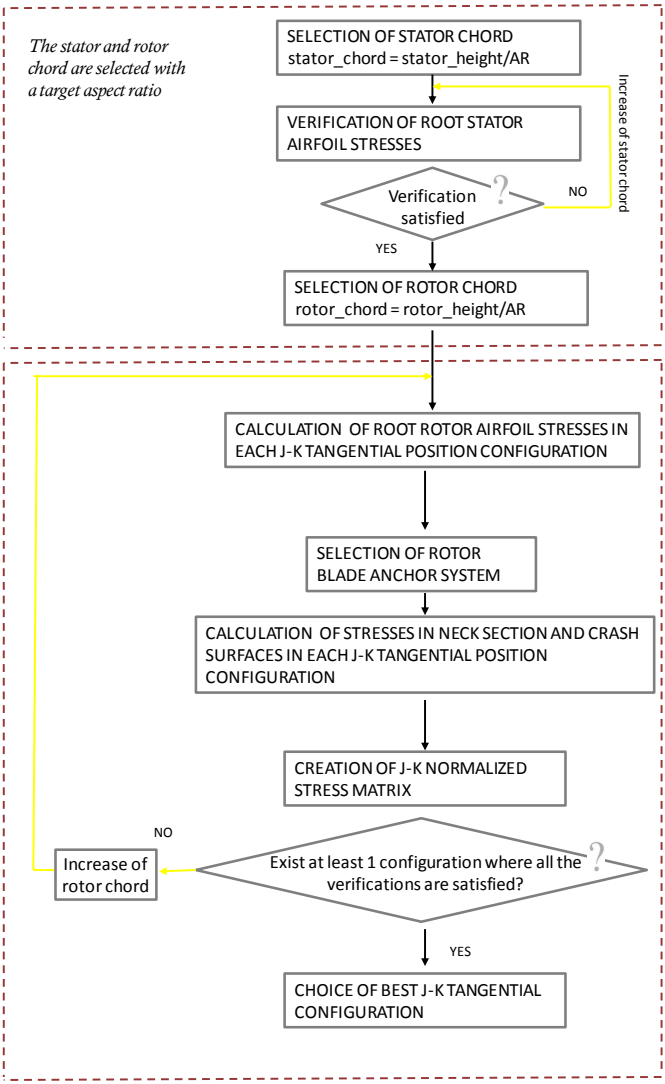

Figure 3.22: New stator chord, rotor chord and anchor system design procedure

3.2 Meridional Flow Path

Turbine design practice is essentially composed of three steps (Havakechian and Greim [8]):

1. optimal choice of the basic design parameters leading to the most efficient flow path
2. the design of most efficient profile sections
3. the employment of advanced three-dimensional features

As we have seen in section 3.1, the second point has been faced with a dedicated optimization aimed at designing a new two-dimensional profile. With reference to point 3, together with the industrial partner we have decided to implement a new prismatic profile (see section 3.1), hence no three-dimensional feature has been employed.

We have then decided to review the rules of the flow path design.

When facing the problem of reviewing the criteria of the meridional flowpath design, it has been at first analysed what are the actual rules, then, taking also into account the new possibilities offered by manufacturing, they have been updated.

3.2.1 Existing meridional flow path design

When the existing design tool faces the problem of meridional flow path shaping, it performs at first the "global"drum meridional flow path design and, at a later time, the single stage meridional flow path design.

Drum meridional flow path design

The existing tool needs only four inputs to perform the shaping of the meridional flowpath in terms of hub inlet diameter

of each stage. The inputs are:

- Drum inlet diameter at hub D_{1H}
- Drum outlet diameter at hub D_{2H}
- Maximum drum inlet stator height H_1
- Maximum drum outlet rotor height H_2

The Drum isentropic enthalpy drop is a given data. In fact the inlet thermodynamic characteristics and outlet pressure are input data.
The design code at the very first iteration takes into account a reference value of drum efficiency η_{drum}. Then the code performs the design of first and last stage, of which the hub diameters and the minimum and maximum height are given data. For the first and last stage the code calculates the enthalpy drop. The choice of the number of stages "Z"is made considering the smallest enthalpy drop between these two:

$$\Delta H_{drum} = \eta_{drum} \cdot \Delta H_{ISO} \tag{3.11}$$

$$Z = \frac{\Delta H_{drum}}{\Delta H_{mimum}} \tag{3.12}$$

Once the number of stages is found, the code calculates the drum axial length with the hypothesis that all the stages have the minimum stage axial length (that is that all the stages present the minimum selectable value of stator and rotor chord).

$$L_{AX} = Z \cdot L_{stage} \tag{3.13}$$

The inlet hub diameter of every intermidiate stage is hence calculated with a simple linear interpolation. An example is reported in Fig.3.23.

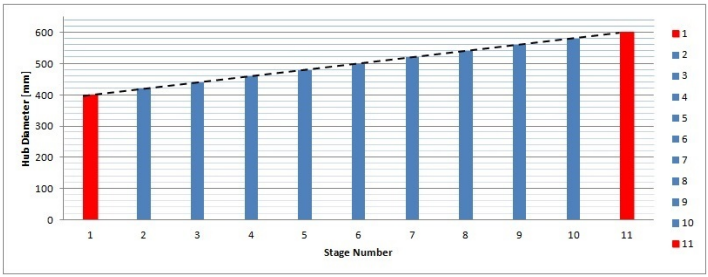

Figure 3.23: Inlet Stage Hub diameter first design

Once the hub diameters are selected, it is possible to design each single stage. The height of each stage is calculated in order to ensure the disposal of the imposed mass flow rate. The tip diameters, and hence the shape of the meridional channel, is the consequence of the thermodynamic expansion and can not be directly controlled by the design engineer.

We have to highligth that the hypothesis that allows the hub diameter to be linear with these shaping rules, is that **all the stages present the same axial length**.

By what we have seen, the stator and rotor chord sizes depend on aspect ratio considerations (we want to target an optimum AR) and mechanical verifications.

What happens in most cases is that the last stages of the drum have bigger chords than first ones. This is due to the lower steam density in last stages, that requires higher blade heights. Higher blade height in fact means bigger chord with the same AR and also:

- Higher centrifugal force
- Higher steam force because of bigger area on which acts the steam pressure

Hence, in most cases the hub meridional channel does not present a linear shaping.

Stage meridional flow path design

Once the first thermodynamic design of the entire drum has been performed, the code makes a detailed thermodynamic analysis of each stage, as it is briefly reported in section 2.1.

It is in this part of the code that the inlet and outlet diameters at hub and tip of stator and rotor are calculated.

The design rules of the code are heavily affected by the **old manufacturing possibilities**.

The basic idea is trying to have a linear growth at the hub between stage inlet and outlet, while at tip the growth is driven by thermodynamic expansion. The old manufacturing imposed, however, the following constraints:

- Stator HUB inlet and outlet diameters must be the same
- Rotor TIP inlet and outlet diameters must be the same

These constraints lead to a "steps"trend of the meridional flow path. The result are a loss in efficiency. An example of this "steps"meridional flow path shaping is reported in Fig. 3.25

3.2.2 New meridional flow path design

Reviewing the rules of meridional flow path design, we have first considered the global drum flow path design, and then the single stage flow path design.

New Drum meridional flow path design

Having a linear shaping of the meridional flow path between inlet and outlet is not an incorrect way to proceed. However,

having only one possible shaping for each couple of values of hub drum inlet D_{1H} and outlet diameter D_{2H} causes a strong reduction of design possibilities.
In fact, a different hub diameter shape leads to different operating conditions for each stage, and hence the thermodynamic expansion will not be exactly the same for the stage. Furthermore, how the hub diameter grows has an impact on axial thrust value, that is an important parameter for mechanical design.

What we wanted was a reliable and easy way to shape the hub diameter that could give to the design engineer the possibility to better exploit the design space. The requirements were:

1. few input parameters
2. a shaping that does not create inflection points
3. a shaping that does not create hub diameter values lower than drum inlet hub diameter
4. a shaping that does not create hub diameter values bigger than drum outlet hub diameter

We have hence decided to use a **quadratic Bezier Curve** that needs only 3 control points.

- 1st point:
  1. first coordinate: drum inlet hub diameter D_{1h}
  2. second coordinate: $x_{1h} = 0$
- 3rd point:
  1. first coordinate: drum outlet hub diameter D_{2h}
  2. second coordinate: $x_h = LAX$ - Drum axial length

- 2nd point:
  1. first coordinate: $D_{intermidiate}$ - a value intermediate between D_{1h} and D_{2h}
  2. second coordinate: $x_{intermidiate}$ - a percentage of drum axial length

The designer engineer has to select only two values: x_{bezier} and y_{bezier}. These values have to be between 0 and 1 and are used for the calculation of the second point coordinates:

$$D_{intermidiate} = D_{1h} + y_{bezier} * (D_{2h} - D_{1h}) \tag{3.14}$$

$$x_{intermidiate} = x_{1h} + x_{bezier} * (x_{2h} - x_{1h}) \tag{3.15}$$

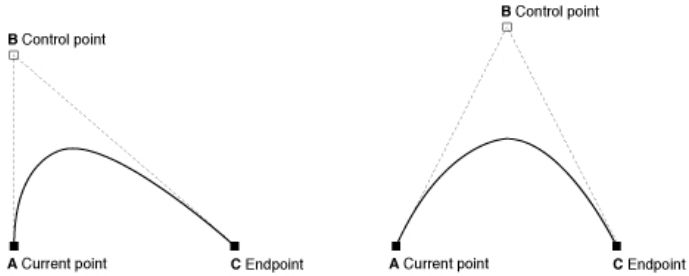

Figure 3.24: Example of quadratic Bezier curve

When $x_{bezier} = 0.5$ and $y_{bezier} = 0.5$ the design follows a linear shaping, as it was in the old design procedure. We have decided to select a Bezier curve because this choice allows having smooth curves, with no inflection points, with the selection of only two input values x_{bezier} and y_{bezier}.

The design engineer has hence the possibility to explore different hub diameter shaping with the same drum inlet and outlet hub diameters.

New Stage meridional flow path design

In implementing the new stage meridional flow path design we have taken into account the new manufacturing possibilities.

The constraints that imposed a "steps" trend to the meridional flow path are not anymore present, given that the new blades will be manufactured with a CNC machine with 5 axis.

We have then decided to shape the stage hub diameter with a linear interpolation. The tip diameter is then calculated with respect to thermodynamic expansion. Limits to maximum flow path opening angles have been chosen.

As we can see in Fig. 3.26, the "steps" trend is not present anymore.

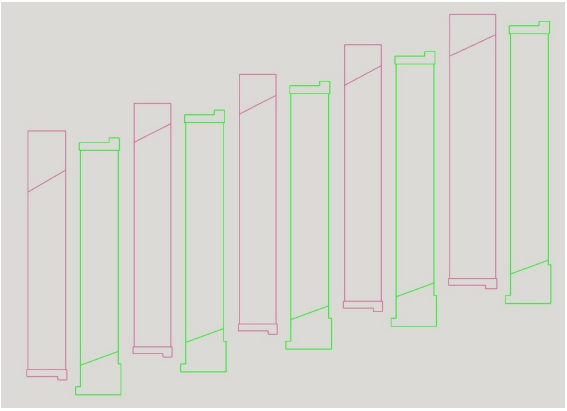

Figure 3.25: Example of old flow path design

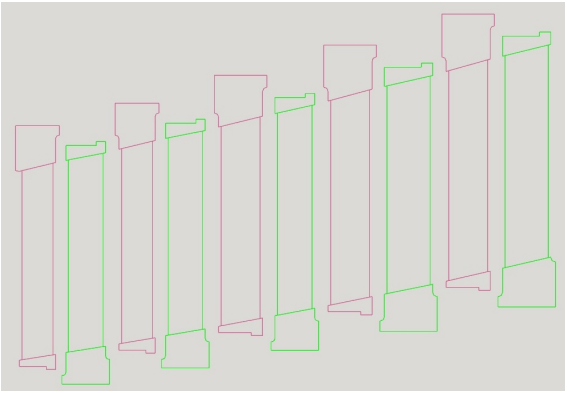

Figure 3.26: Example of new flow path design

Chapter 4

Integration in the Production Process

This chapter provides a description of how the integration of the 1-D design tool with the subsequent phases has been maintained and enhanced

As we have seen in the introduction, the integration of the tool with the subsequent phases of the industrial production process was an essential requirement to the present work.

The existing tool provides the data for the phases relative to the generation of:

1. 3D Master Model
2. 2D Drafting Tables
3. Assembly Tables
4. Groove tables

It has been necessary to review all these data in order to have the same integration with the subsequent phases of the production process.

4.1 Data for 3D Master Model

The data for 3D master model are provided with 2 output files: the first is relative to stator 3D blade, the second is relative to rotor 3D blade. In both cases it is modelled also the anchor system, that is an integral part of the blade. These output files have been realized together with the industrial partner in order to directly speak with the CAD software used in the company. Hence, it is possible having a 3D CAD model of the blades in one single step.

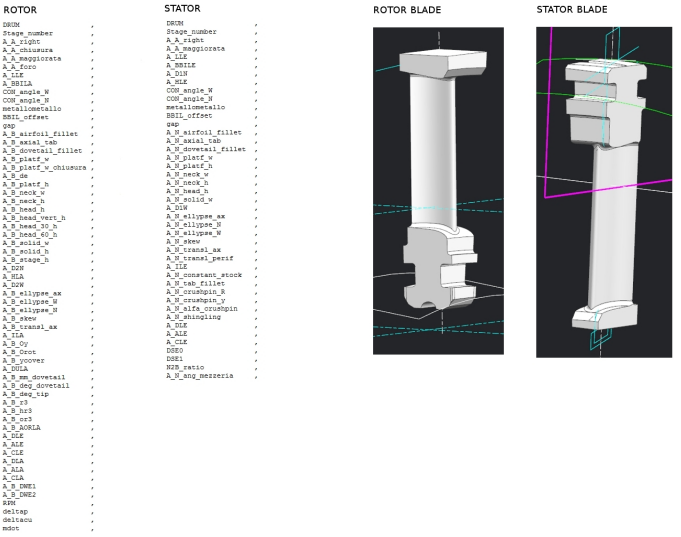

Figure 4.1: Example of 3D Master Model and the data text generated by 1D code

This procedure, fast and reliable, allows the designer to have a 3D model of the blades useful for further analysis of the blade or anchor system, especially in terms of stress with FEM instruments.

Together with the industrial partner, the rotor 3D master model data output of the tool have been updated and reviewed according to new design, and at the same time it has been introduced the files relative to 3D modelling of stator blade, not present in the old version of the code.

4.2 Data for 2D Drafting Tables

With reference to the data necessary for 2D drafting tables, they have been updated according to the new design. In Fig. 4.2 it is reported an example of the output data and the 2D drafting table generated with these last ones.

4.3 Data for Assembly Tables

By the moment that, in order to take advantage of the new manufacturing possibilities, the design of rotor and stator anchor systems have been reviewed, the assembly system has been deeply modified.

It has then been necessary reviewing all the output data for assembly. In figures 4.3 and 4.4 are reported two examples of Rotor and Stator assembly tables so generated.

4.4 Data for Groove Tables

Respect to past design procedure, it has been decided to add a new output relative to groove tables. This new output is intended to help the assembly procedure.

All these outputs, made to directly speak with CAD instruments, are time saving for the design engineer and increase the robustness of the product development process.

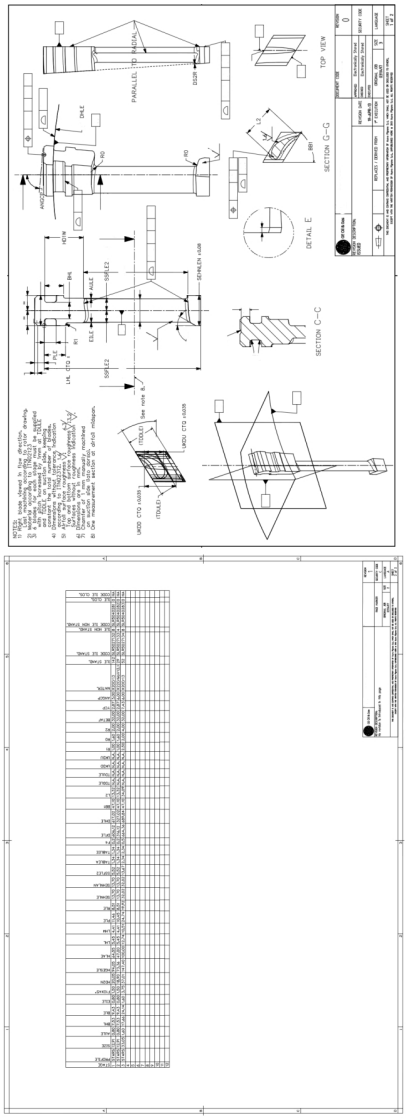

Figure 4.2: Example of 2D Drafting Table

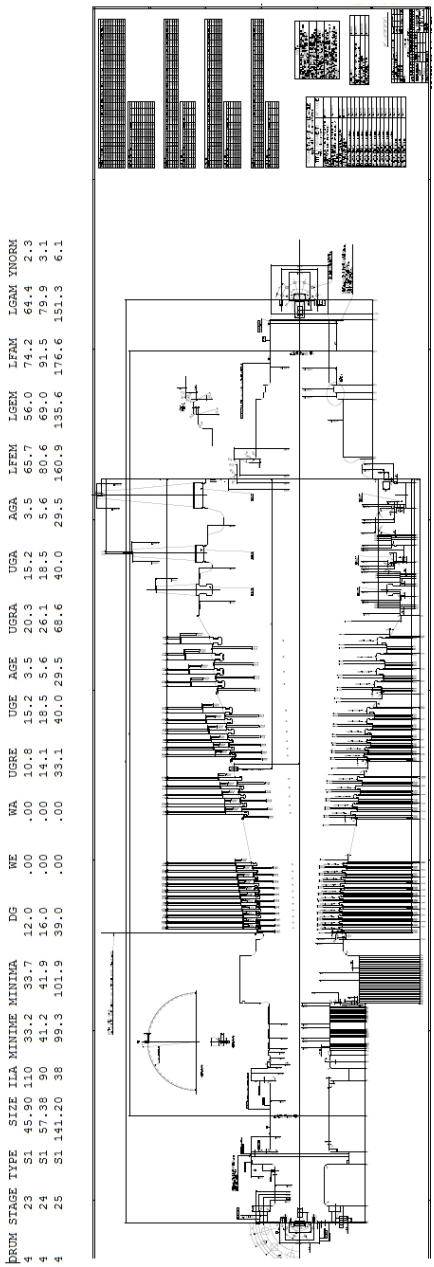

ROM	STAGE	TYPE	SIZE	ILA	MINIME	MINIMA	DG	WE	WA	UGRE	UGE	AGE	UGRA	UGA	AGA	LFEM	LGEM	LFAM	LGAM	YNORM
4	23	S1	45.90	110	33.2	33.7	12.0	.00	.00	10.8	15.2	3.5	20.3	15.2	3.5	65.7	56.0	74.2	64.4	2.3
4	24	S1	57.38	90	41.2	41.9	16.0	.00	.00	14.1	18.5	5.6	26.1	18.5	5.6	80.6	69.0	91.5	79.9	3.1
4	25	S1	141.20	38	99.3	101.9	39.0	.00	.00	33.1	40.0	29.5	68.6	40.0	29.5	160.9	135.6	176.6	151.3	6.1

Figure 4.3: Example of Rotor assembly Table

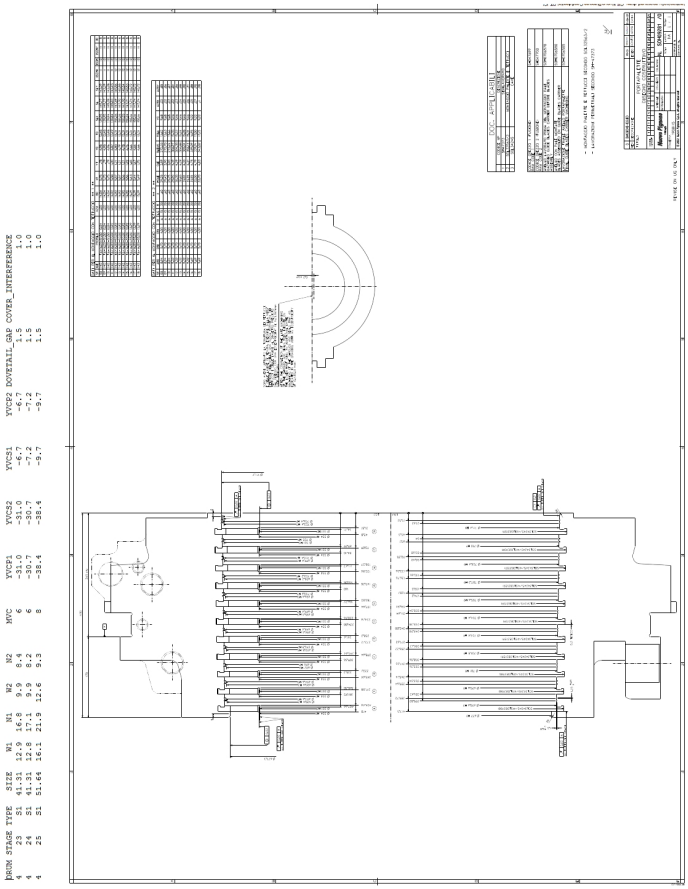

Figure 4.4: Example of Stator assembly Table

Chapter 5

New Design Turbines

This chapter provides a description of two steam turbines designed with the updated design tool

In this chapter are reported three cases of drums realized with the updated design code.

Real machines, designed with the old tool and yet produced and operating, have been re-designed with the new code.

So, given the same input file used for the past design, the updated tool has designed new design machines.

A CFD analysis both of the old existing drums and of the new ones has been made.

The results have been used in order to :

- Verify the increase in efficiency respect to old design
- Verify performance predicted by the one-dimensional tool

5.1 Turbine N1

The first turbine analysed is a turbine composed of:

- 1 Impulse stage for partialisation
- 5 Reaction drums
- 1 Low pressure drum

Given the same input used for existing machine, a new machine has been designed with the updated code. The new design uses the optimized profile sections and the new flowpath design, as well as the optimized relative tangential positioning of rotor cover, blade and foot.

We have decided to analyse with CFD three-dimensional steady calculation (Full Navier Stokes) the first and fourth drum. We have chosen the first and fourth ones because they are characterized by different values of aspect ratio and radius ratio, that, as we have seen in section 3.1.2, have a strong impact on row efficiency.

In Fig. 5.17 it is reported a schematic design of the turbine output of the old code, while in 5.15 is reported the design of the same turbine using the updated code (new profile section, new flowpath design).

The input data used for the design are the same, hence the two designs respect the same constraints and requirements.

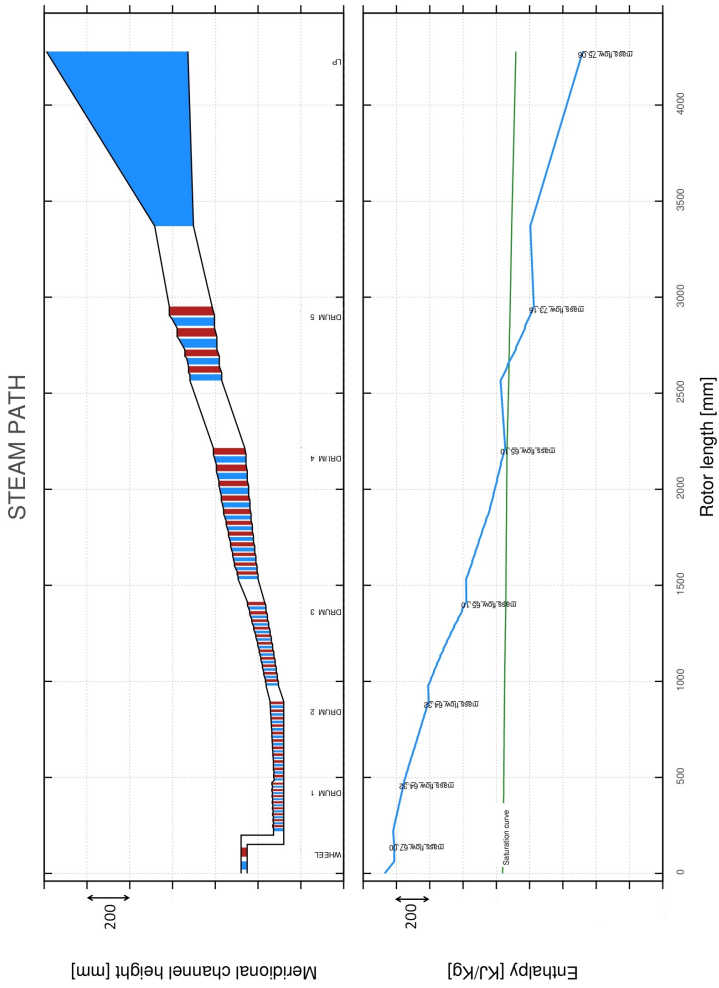

Figure 5.1: Turbine N1 old Design

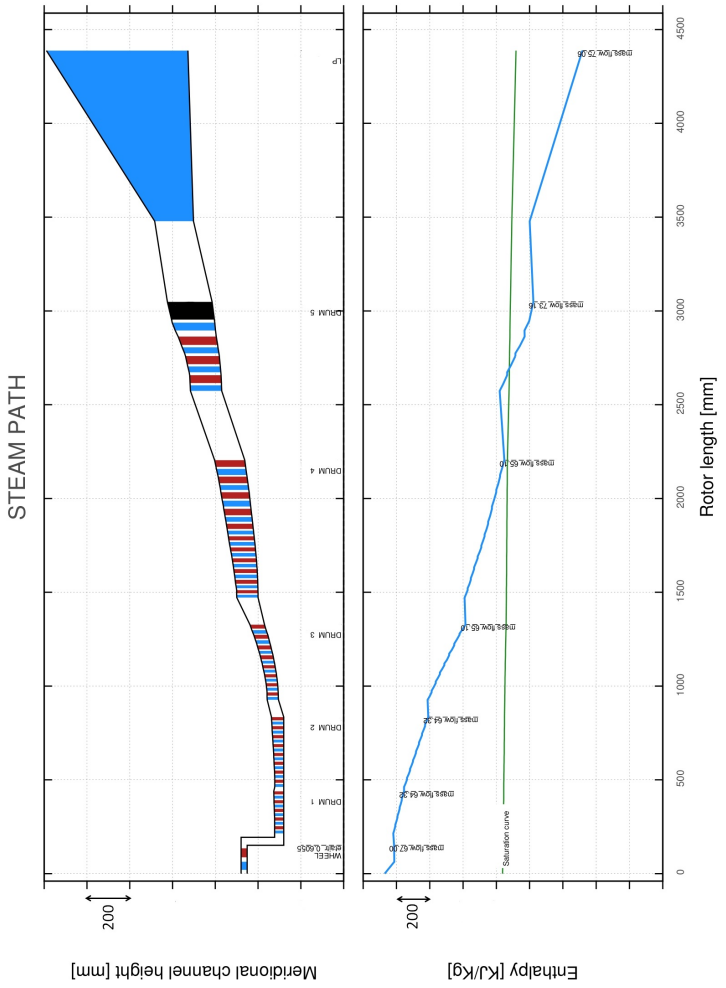

Figure 5.2: Turbine N1 new Design

5.1.1 Turbine N1: First Drum

With reference to the first drum (Fig. 5.3) we have that the new design presents a reduced axial length. The load coefficient at which the new blades work is higher than the one relative to old design.

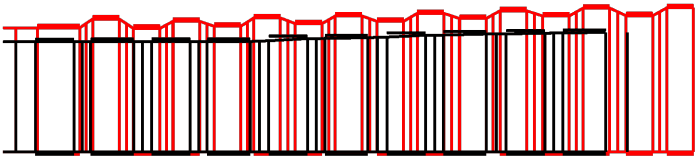

Figure 5.3: Comparison between old (red) drum design and new (black) drum design

In fact, as we have seen in chapter 3 ,the higher nominal stagger and the smaller radius of curvature of the uncovered part of the suction side of GEO-2-new design respect to GEO-1-old design, together with higher pitch-to-axial chord ratio, provide an increase in the blade loading. In particular, we can notice a reduction in the number of stages (8 in the old design, 5 in the new one), and each stage presents a bigger chord, associated to the higher stresses connected to an higher load.

By the moment that the target of the present work was having more efficient turbines, we have at first run CFD simulations. The CFD three-dimensional steady calculation (Full Navier Stokes) have been performed by means of the multi-row, multi-block version of the TRAF code (Arnone [2],Arnone [3]).

Both the old design drum and the new one have been analysed. The results in terms of total-to-total efficiency seen by TRAF code and relative to the two drums are reported

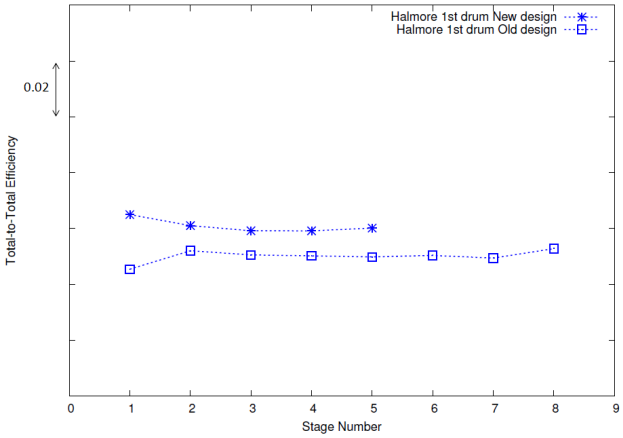

Figure 5.4: Comparison between old drum design and new drum design in terms of total-to-total efficiency (CFD - TRAF code)

in Fig. 5.4. What we can notice is that the target in term of efficiency increase has been satisfied (about 1% for each stage). Together, we can see an increase in the load, that has lead to a strong reduction in stage number (Fig. 5.5). This growth in stage load is due to the higher nominal stagger of the new blade profile and also to the fact that the new stage length has been increased respect to the old one. The effect is hence often a reduction in stage number in order to match the maximum drum length.

At the same time an important requirement to the updated code was his reliability in drum efficiency calculation. In fact the code is used for routine design and the efficiency output of the code is used as a criterion for the selection of a turbine configuration respect to another. It is hence essential having a reliable prevision. In figures 5.6,5.7 and 5.8 it

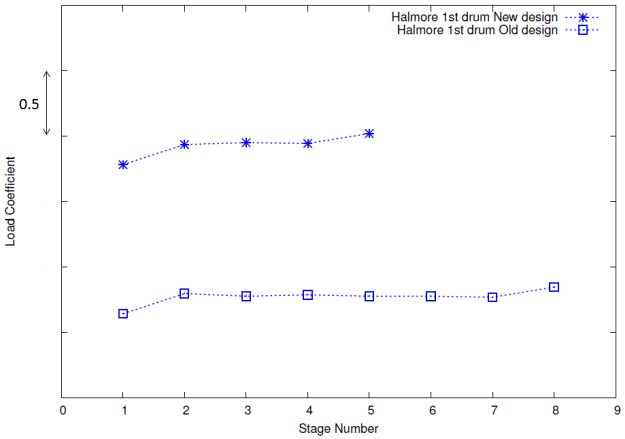

Figure 5.5: Comparison between old drum design and new drum design in terms of load coefficient (TRAF code)

is reported the comparison in terms respectively of flow coefficient, load coefficient and total-to-total efficiency between the 1-D code calculation and the TRAF code one. We can see a good match in terms of efficiency and flow coefficient. In fact, a good prevision in terms of efficiency, and hence a proper design of the stages, leads to a correct flow coefficient calculation and hence to a correct estimation of the power developed by each drum .

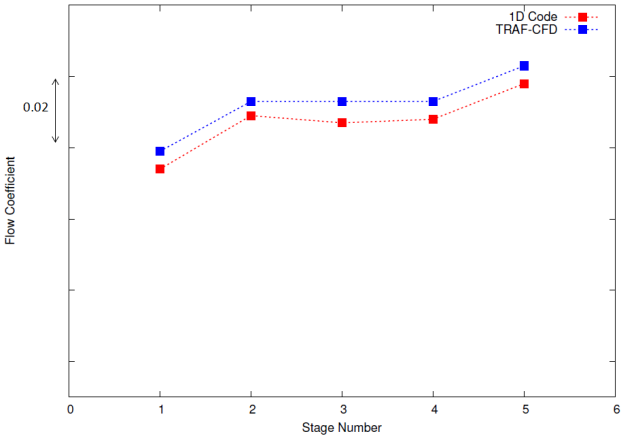

Figure 5.6: Comparison in terms of flow coefficient seen by 1-D design code and TRAF code

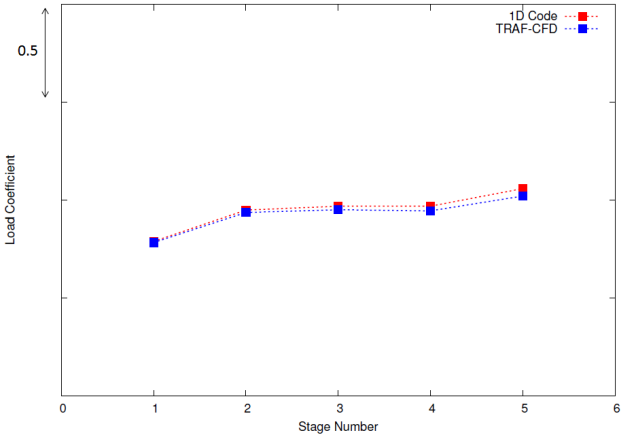

Figure 5.7: Comparison in terms of load coefficient seen by 1-D design code and TRAF code

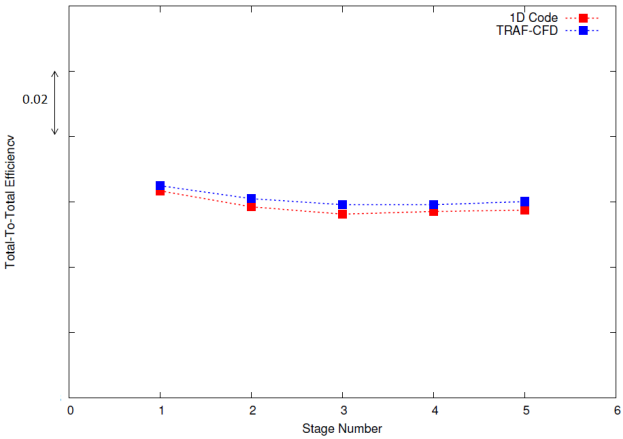

Figure 5.8: Comparison in terms of efficiency seen by 1-D design code and TRAF code

5.1.2 Turbine N1: Fourth Drum

The fourth drum of the turbine N1 is characterized by higher Aspect Ratio and Radius ratio respect to the first drum. The analysis has been analogous to the one made for the first drum.

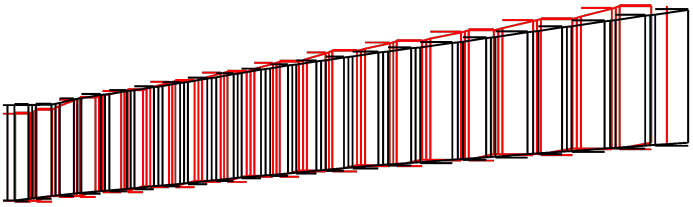

Figure 5.9: Comparison between old (red) and new (black) drum design

At first we have run CFD calculation in order to verify the efficiency increase connected with the new design. In this drum too we see an increase in efficiency (about 1% for each stage), while the load coefficient is almost the same both for new design and old one. Respect to the drum number 1, we see here that old design and new design have the same number of stages and a similar drum axial length. The two turbine are working almost in the same operating point and we can appreciate the increase in efficiency connected to the new profiles. Even if the new profile is more weak in terms of mechanical resistance than the old one, the chords selected by the code are similar to the ones chosen in the old design. This has been possible for the rotor through the optimization of the tangential positioning of cover and anchor system respect to blade (see section 3.1.4).

With reference to figures 5.12, 5.13 and 5.14, we can see a

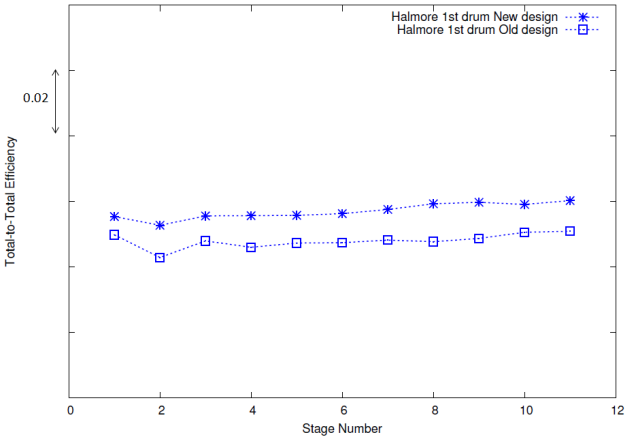

Figure 5.10: Comparison between old and new drum design in terms of total-to-total efficiency (TRAF code)

good agreement between CFD and 1D code calculation, even if the discrepancy between the two tools is slightly bigger than in the previous drum (see Fig.5.8). This is probably due to a stronger impact of secondary flows on main flow rate that is difficult to be modelled with a correlative approach.

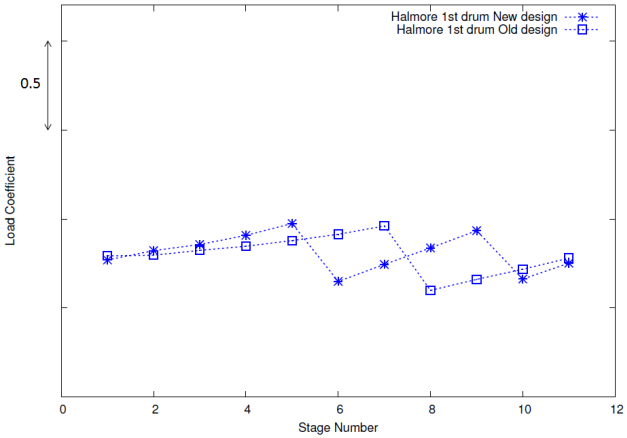

Figure 5.11: Comparison between old and new drum design in terms of load coefficient (TRAF code)

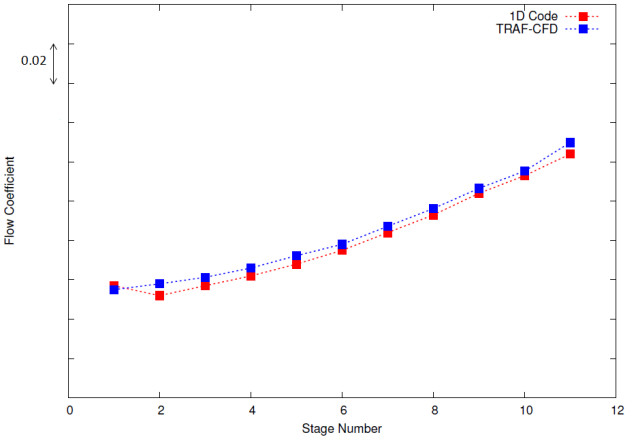

Figure 5.12: Comparison in terms of flow coefficient seen by 1-D design code and TRAF code

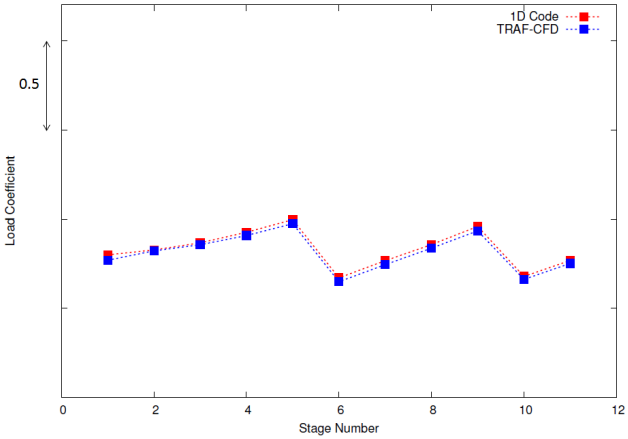

Figure 5.13: Comparison in terms of load coefficient seen by 1-D design code and TRAF code

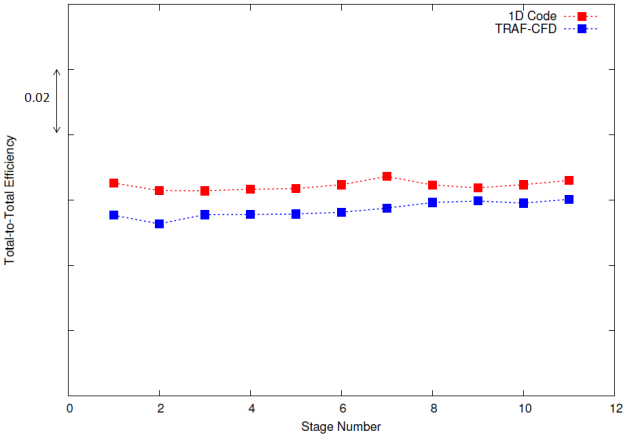

Figure 5.14: Comparison in terms of total-to-total efficiency seen by 1-D design code and TRAF code

5.2 Turbine N2

The second turbine analysed is a turbine composed of:

- 1 Impulse stage for partialisation
- 5 Reaction Drums
- 1 Low pressure drum

5.2.1 Turbine N2: First Drum

We have analysed the first drum.

At first we have run CFD calculation in order to verify the efficiency increase connected with the new design. In this drum we see an increase in efficiency, while the load coefficient is higher in new design respect to old one.

We see here in fact that new design has less stages then old design, even if the drum axial length is comparable.

As we have seen, the new stage axial length is bigger then the old one. Hence, when the maximum axial length is a strong constraint, the new design tends to have a lower number of stages respect to old one. This leads to stages more loaded in average respect to old ones.

Even if the new design turbine is working at an higher load coefficient, we can appreciate anyway the increase in efficiency connected to the new profile section.

In fact, when the optimization procedure for the new prismatic profile choice has been performed, one of the requirement was having more efficient profiles at an higher load respect to old one (see section 3.1.1).

With reference to figures 5.20,5.21 and 5.22, we can see a good agreement between CFD and 1D code calculation.

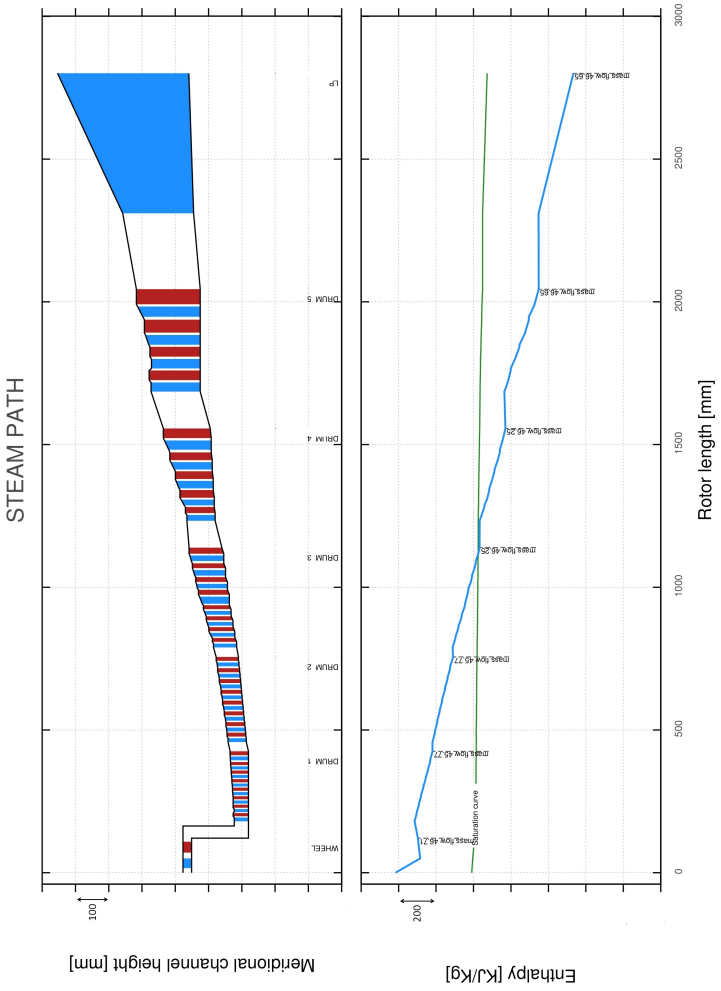

Figure 5.15: Turbine N1 old Design

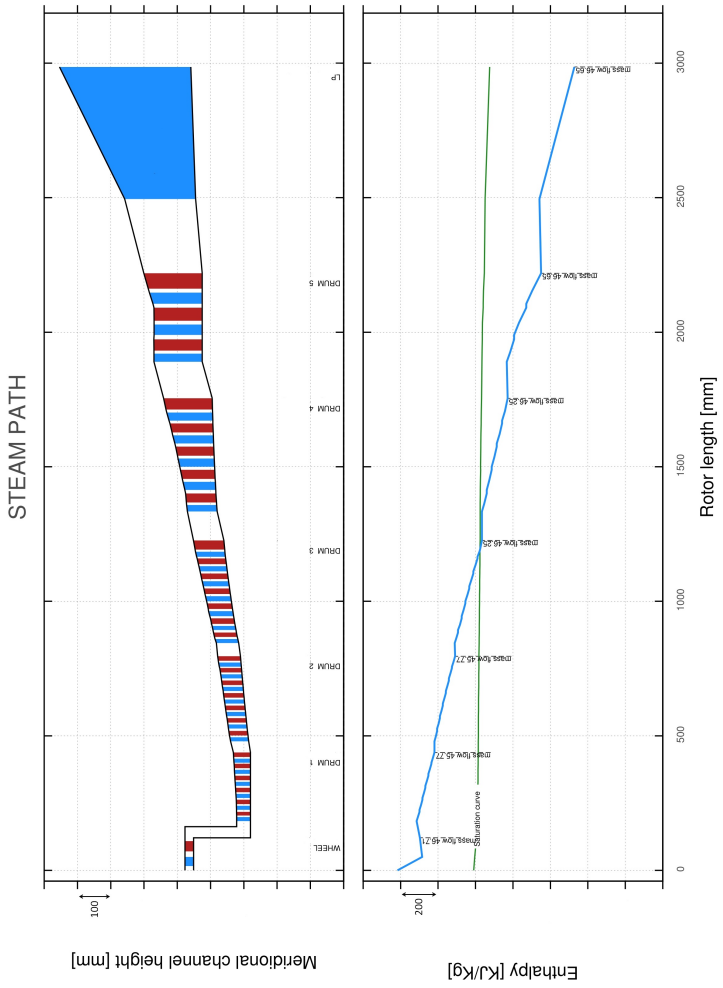

Figure 5.16: Turbine N1 new Design

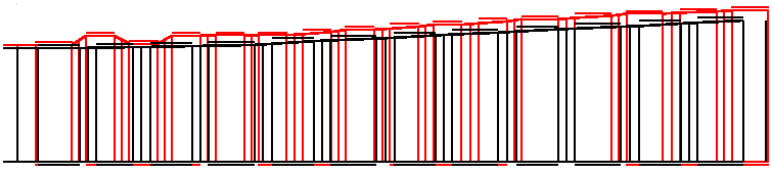

Figure 5.17: Comparison between old (red) and new (black) drum design

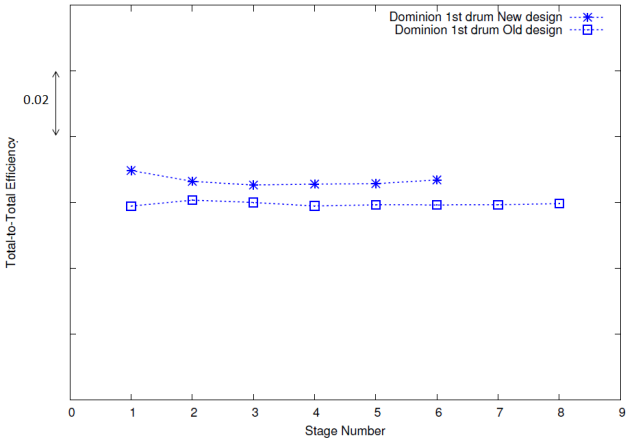

Figure 5.18: Comparison between old and new drum design in terms of total-to-total efficiency (TRAF code)

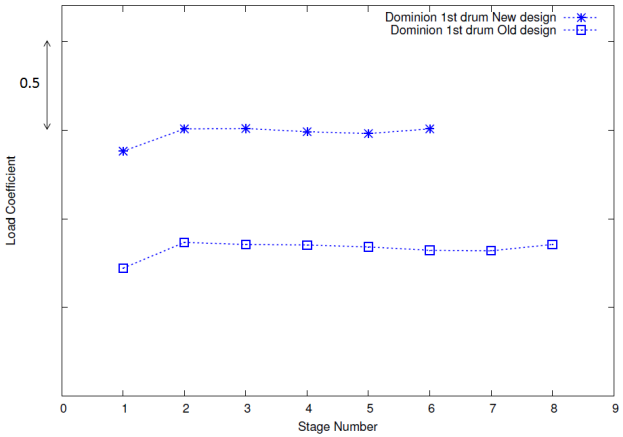

Figure 5.19: Comparison between old and new drum design in terms of load coefficient (TRAF code)

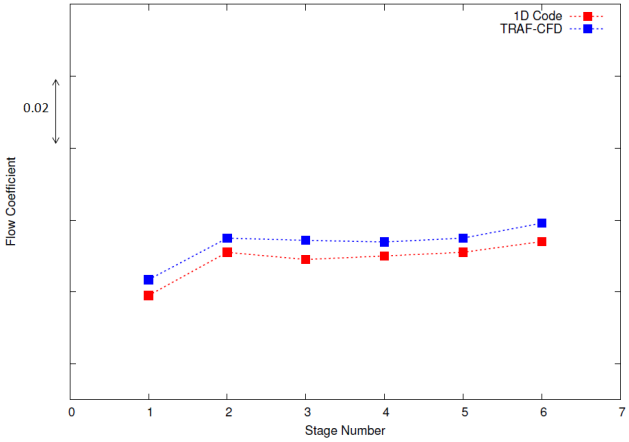

Figure 5.20: Comparison in terms of flow coefficient seen by 1-D design code and TRAF code

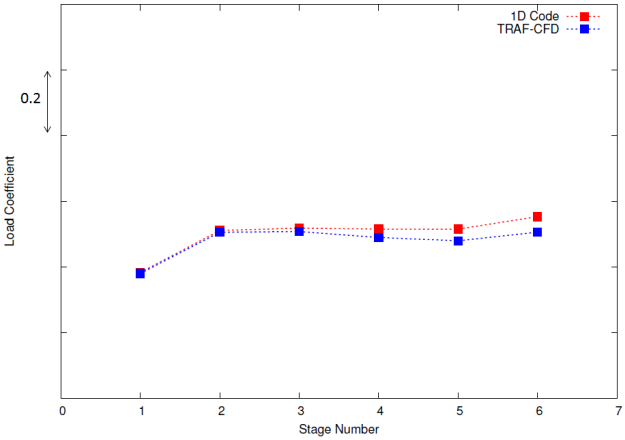

Figure 5.21: Comparison in terms of load coefficient seen by 1-D design code and TRAF code

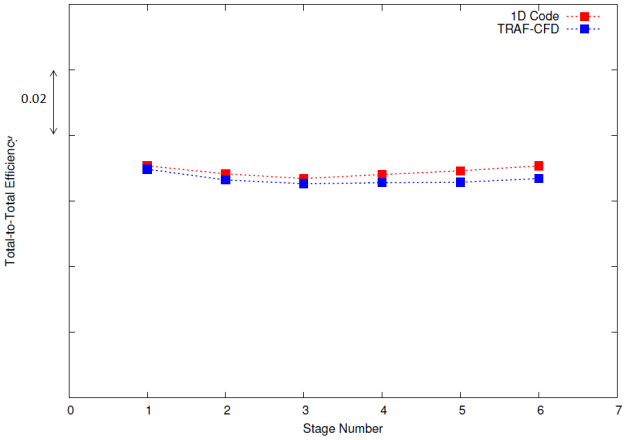

Figure 5.22: Comparison in terms of total-to-total efficiency seen by 1-D design code and TRAF code

Conclusions

The present Ph.D. research program has been developed in the framework of an industrial research program. The purpose of this industrial project was obtaining an efficiency increase of the company's steam turbines.

One of the requirement of the present program was also continuing to use the existing industrial design tool. This tool performs both a thermodynamic and mechanical design. Given few inputs selected by the designer with a front-end interface the tool designs a complete 50% reaction drum. The analysis carried out can be divided into a mean line thermodynamic analysis and a section where mechanical verifications are performed.

In order to achieve an higher efficiency level, we have individuated as key factors the **profile sections**, the choice of the basic design parameters leading to the **meridional flow path** and the **seal design**.

We have decided to investigate the first two factors, while the third one has been dealt by the industrial partner.

The existing code is based on a "Direct Problem"approach. Hence, given a profile shape, the code has the task to design a turbine where this profile works at his best efficiency point.

We have decided to maintain the existing design philosophy and find a new more efficient profile. The new profile geometry has been obtained through a multi-objective, aero-

dynamic optimization (Bellucci et al. [5]). The overall optimization strategy relies on a neural-network based approach.

Even if during the last decade the major steam turbine manufacturers have devoted significant investment on advanced three-dimensional blading design, together with the industrial partner it has been chosen to follow a more conservative path with respect to what it is actually implemented and to find an optimized new prismatic profile. In fact with the latest generation of two-dimensional constant profile section blading it has been recorded a reliable operation and outstanding performance in the entire range of setting angle, aspect ratio and stage loading (Havakechian and Greim [8]). In order to implement the new profile into the code, a correlative approach has been tuned in order to better model the new profile performance.

An important and interesting step has been the problem of the tangential positioning of the rotor blade respect to cover and foot (rotor anchor system). Respect to what was implemented, now the consequences in terms of stresses connected to a tangential positioning respect to another have been taken into consideration. We have hence thought that it could be possible to use this positioning to reduce the stresses acting on the critical sections. A new routine has been implemented that performs the research of the "optimum position"in terms of stresses. This has lead to smaller rotor chords with the same operating conditions, with all the consequent advantages.

The second step has consisted in reviewing the rules of the flow path design. When facing the problem of reviewing the criteria of the meridional flowpath design, it has been at first analysed what are the actual rules, then, taking also into account the new possibilities offered by manufacturing, they have been updated. We have at first considered the drum flow path design and then the single stage flow path design.

In order to give one more degree of freedom to the de-

sign engineer, instead of having only the linear option for drum hub diameter shaping, we have decided to implement a quadratic Bezier Curve with 3 control points.

In implementing the new stage meridional flow path design we have taken into account the new manufacturing possibilities.

The constraints that imposed a "steps" trend to the meridional flow path are not anymore present, given that the new blades will be manufactured with a CNC machine with 5 axis.

We have then decided to shape the stage hub diameter with a linear interpolation.

Another constraint to the present work was maintaining not only the existing design tool, but also the integration of the tool with the subsequent phases of industrial production process. This part has not only been maintained but has been enhanced.

At last, in order to validate the new design tool, real machines, designed with the old tool and yet produced and operating, have been re-designed with the updated code. So, given the same input file used for the past design, we have had new machines as output. A CFD analysis both of the old existing drums and of the new ones has been made. We have been able to see that the target in term of efficiency increase has been satisfied. At the same time in two of the three cases we have seen an increase in the load, that has lead to a strong reduction in stage number. This growth in stage load is due to the higher nominal stagger of the new blade profile and also to the fact that the new stage length has been increased respect to the old one. The effect is hence often a reduction in stage number in order to match the maximum drum length.

At the same time an important requirement to the up-

dated code was his reliability in drum efficiency calculation. In fact the code is used for routine design and the efficiency output of the code is used as a criterion for the selection of a turbine configuration respect to another. In all three cases we have seen a good match in terms of efficiency and flow coefficient between 1D tool and CFD performance. Hence, the 1D tool can be used for the selection of the most promising design.

Bibliography

[1] D G Ainley and G C R Mathieson, *An examination of the flow and pressure losses in blade rows of axial flow turbines*, **2891** (1955).

[2] A Arnone, *Viscous analysis of three–dimensional rotor flow using a multigrid method*, ASME J. Turbomach. **116** (1994), no. 3, 435–445.

[3] A. Arnone, *Multigrid methods for turbomachinery navier–stokes calculations*, Solution Techniques for Large–Scale CFD Problems (W. G. Habashi, ed.), John Wiley & Sons, 1995.

[4] Ronald H Aungier, *Turbine aerodynamics: Axial-flow and radial-flow turbine design and analysis*, ASME New York, 2006.

[5] J bellucci, F Rubechini, A Arnone, L Arcangeli, N Maceli, and V Dossena, *Optimization of a high-pressure steam turbine stage for a wide flow coefficient range*, Proceedings of ASME Turbo Expo 2012, 2012.

[6] M W Benner, S A Sjolander, and S H Moustapha, *Influence of leading-edge geometry on profile losses in turbines at off-design incidence: Experimental results and an improved correlation*, **119** (1997), 193–200.

[7] H R Craig and H J Cox, *Performance estimation of axial flow turbines*, (1970-71), Vol.185 32/71.

[8] S Havakechian and R Greim, *Aerodynamic design of 50 per cent reaction steam turbines*, Proceedings of the Institustion of Mechanical Engineers, vol. 213, 1999, p. Part C.

[9] S C Kacker and U Okapuu, *A mean line prediction method for axial flow turbine efficiency*, **115** (1982), 621–656.

[10] S H Moustapha, S C Kacker, and B Tremblay, *An improved incidence losses prediction method for turbine airfoils*, **112** (1990), 267–276.

[11] A Stodola, *Die dampfturbinen und ihre aussichten als warmekraftmaschinen*, Springer-Verlag, Berlin, 1903.

[12] A. Stodola, *Dampf und gas turbinen*, Springer-Verlag, Berlin, 1922.

[13] W Traupel, *Thermische turbomaschinen zweiter band gelnderte betriebsbedingungen, regelung, mechanische probleme, temperatur probleme*, Springer-Verlag Berlin heidelberg New York, 1977.

[14] C Wu and C Brown, *A theory of the direct and inverse problems of compressible flow past cascade of arbitrary aerofoils*, Journal of the Aeronautical Sciences **19** (1952), 183–196.